THE UNIVERSITY OF MICHIGAN

COLLEGE OF LITERATURE, SCIENCE, AND THE ARTS

Department of Physics

Final Report 032150-F-1

IONIZATIONAL RELAXATION IN SHOCK-HEATED MERCURY VAPOR

James Harvey Dell

Otto Laporte, Project Supervisor

Michael Sanders, Project Supervisor

ORA Project 032150

under grant from:

AIR FORCE OFFICE OF SCIENTIFIC RESEARCH
Grant No. AF-AFOSR-70-1849
ARLINGTON, VIRGINIA

administered through:

OFFICE OF RESEARCH ADMINISTRATION - ANN ARBOR

January 1972

IMRQ614

ABSTRACT

This paper is concerned with aspects of the ionizational relaxation in a shock-heated mercury plasma. A uniformly heated, pressure-driven shock tube was used to produce 4200 °K to 12,000 °K mercury plasmas in which the relaxation process was studied. The total plasma luminosity was observed using a photomultiplier tube, with the time of shock passage and the shock velocity established using a schlieren optical system.

It is shown that the ionizational relaxation time depends inversely on the initial vapor pressure or atom number density, and directly on the final electron number density. The final plasma temperature is shown to be more relevant for strongly ionized shocks than the commonly used ideal gas temperature.

Ionizations caused by electron-atom collisions appear to occur as a single step rather than by cumulative steps as atom-atom collision ionizations.

A previously unobserved feature of ionizational relaxation has been detected. The luminosity profile shows two distinct points at which the slope of the curve changes abruptly. No explanation of this feature could be found.

Radiation overshoot is shown to be an effect which occurs at low impurity levels. The true relaxation time corresponds to the end of the overshoot phenomenon. Impurities are seen to affect the shape of the relaxation profile greatly, and manometer and vacuum pump oils are shown to be possible sources of impurities in some previous studies.

ACKNOWLEDGEMENTS

I wish to express my appreciation to Professor Otto Laporte for initiating the present research and for his help and advice through the initial stages of this research. I would like also to thank Dr. T. Michael Sanders for assuming chairmanship of my doctoral committee after Professor Laporte's untimely death.

I extend special thanks to Dr. M. John Yoder. His suggestions and criticism concerning the design modifications for the heated shock tube and experimental procedures were very helpful. My thanks also to Dr. C. Wilbur Peters, Dr. Richard D. Sacks and Dr. Yukio Tomozawa.

I would also like to thank my wife, Dr. Carol I. Dell for her help in data reduction and in the preparation of this manuscript.

Financial support for this research was supplied by the United States Air Force Office of Scientific Research.

TABLE OF CONTENTS

LIST OF FIGURES

List of Figures (con't).

CHAPTER I

INTRODUCTION

1. Elementary Shock Theory

A simple pressure-driven shock tube consists of a long tube of uniform cross-section, divided into two chambers by a breakable diaphragm. The expansion chamber contains a test gas at low pressure (1 to 100 Torr usually). The compression chamber is slowly filled with a "driver" gas until the diaphragm bursts (100 to 2000 psi) and the driver is released into the expansion chamber. Diaphragm thickness, material, and the depth of grooves scored on the diaphragm face control the bursting pressure.

If the expansion of the driver into the low pressure chamber is supersonic relative to the test gas, then the gas far ahead of the driver remains at rest in its initial state (P_0, T_0, ρ_0), until the instant it is "shocked". Diffusion between the two gases is so extremely slow compared to the shock processes that all mixing may normally be ignored. Therefore, the interface between the gases acts similar to a solid piston, moving at uniform speed and sweeping up the test gas ahead of it.

The test gas is compressed and accelerated until it has the same pressure and speed as the interface, but the actual pressure change in the test gas moves forward even faster than the interface. This sudden pressure step in the test gas is the shock front.

When the diaphragm bursts, the desired single sharp step in pressure, extending uniformly across the entire cross-section, will not normally occur. A single plane pressure discontinuity will result, however, after the pressure change has moved forward 20 to 50 tube diameters. Pressure variations perpendicular to the flow will obviously come to an equilibrium very quickly as the interface and shock front move forward. Pressure variations along the tube axis will act as a series of pressure pulses following one another. The gas will be heated by the rapid compression due to the passage of the first pressure pulse. The velocity of sound (or pressure change) increases as the square root of the absolute temperature, so that, a following pulse will travel faster than the first. Therefore, a second pulse will overtake the first and combine with it to form a single large pulse. Similarly, all gradual variations in pressure will steepen as the tail of the variation overtakes the head, until a pressure discontinuity results. A more detailed description of how irregularities in pressure converge to form the shock front has been given by Laporte[1].

In the compression section a rarefaction wave travels back into the driver gas, but because conditions here are the reverse of those occurring in the test section, this wave gradually disperses along the tube as it moves.

The "shocked" gas, which has all undergone exactly the same compression process in reaching its final state

(P_1, T_1, ρ_1), forms a slug of gas at uniform high temperature and pressure. This slug of plasma, between the interface and the shock front, moves at the speed of the interface and lengthens as more gas collects at the shock front. Because there is a Boltzmann distribution over the excited atomic and molecular states, and an equilibrium of energy among the degrees of freedom of the system, this plasma is usually referred to as being in "local thermodynamic equilibrium" (L.T.E.).

The uniformity of this plasma and the existence of L.T.E. make it excellent as a spectroscopic source, or for studies of supersonic flows[2]. Measurements of transition probabilities (gf values) for optical frequencies[3], and the broadening of spectral lines[4,5], have been particularly successful using shock tubes.

To the particles in the plasma, the tube end-wall appears as a piston rushing toward them at supersonic speed. Therefore, when this plasma slug meets the end-wall a new shock front will form and travel back through the slug, compressing and heating the gas still further. Similarly, this shock wave will be reflected when it strikes the interface. This second reflection is not generally as good as the first, however, because the interface is slightly diffuse due to some mixing of the driver and test gases.

The gas plasma (in L.T.E.) behind each shock may be used for study purposes, but the time for observation gets progressively shorter behind each reflection. The observation

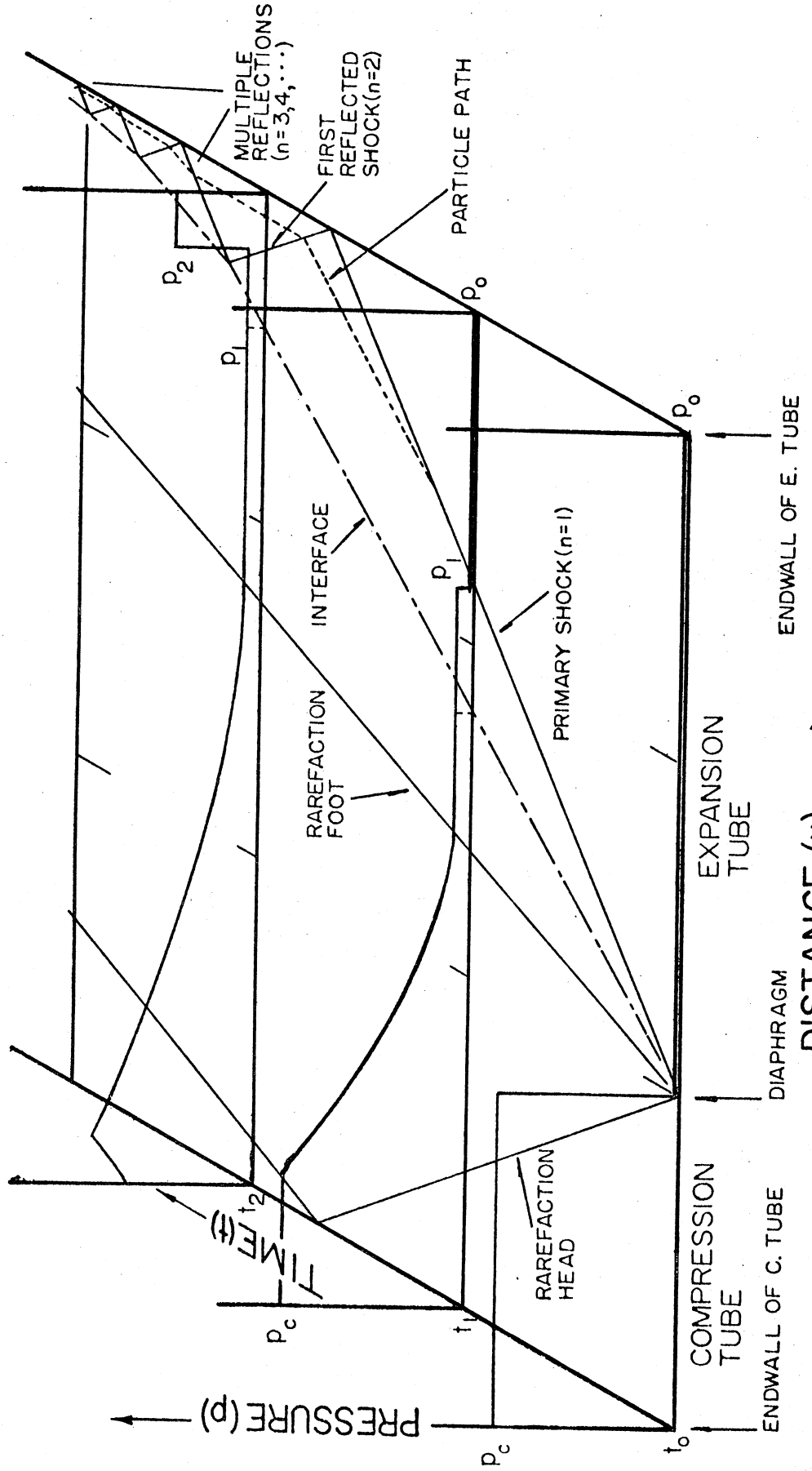

Figure 1. x-t-P diagram

time available is from the passage of the shock front until the arrival of either the interface or the next reflected shock. For this reason, studies are commonly limited to the primary or first reflected shock regions.

Figure 1 illustrates all of these actions graphically[6].

2. Boundary Layers

For the hot plasma moving at supersonic speed, energy loss by the gas molecules and viscous drag occur at the cold tube wall. The combination of cooling and drag results in the growth of a cooler, slower moving "boundary layer" along each wall, and shock front deceleration is possible.

The boundary flow is usually very thin and laminar near the shock front, and becomes thicker and turbulent nearer to the interface. As shock strength increases the layer will often become thicker, and turbulence will begin earlier. Boundary layers in mercury vapor have been observed to grow to such an extent that the tube is completely choked off and only a supersonic turbulent flow results.

The available observation time will be shortened because material is removed from the plasma and flows back through the boundary layer to mix with the driver gas. When observations are analyzed, the presence of a boundary layer must not be forgotten, because observed phenomena may actually be in this layer, not in the uniform plasma being studied.

3. Radiation

For extremely luminous shocks the energy lost by radiation can become very significant and true thermodynamic equilibrium may not actually occur. Since the plasma is optically quite thin, radiation easily escapes from the system with a resulting rapid energy loss. The temperature and luminosity decrease toward the tail of the slug, accompanied by adjustments in the other gas variables such as density and number of free electrons, etc. The decrease in the total energy of the plasma gas with time, caused by radiation losses is known as radiation decay.

Radiation decay has been observed for many gases, either for very strong primary shocks, or for the reflected shocks. Tumakaev and Lazovskaya[7] have studied the very pronounced decay which occurs for only moderately strong shocks in mercury vapor. Their observations will be discussed further in connection with the present study of mercury vapor.

4. Relaxations

Ideally the passage of the shock front instantaneously adds energy and compresses the stationary test gas, causing the gas to change from its initial condition (P_0 , ρ_0 , T_0) to some new equilibrium condition (P_1 , ρ_1 , T_1). However, the only efficient mechanism available to distribute the added energy among the available energy states and bring about final equilibrium, is collisions between gas molecules.

The time between collisions is not infinitesimal, and

many collisions will be necessary to bring about equilibrium, therefore, the change in the state of the gas cannot occur instantly. This delay was first observed at Michigan by Turner in 1956[4], but the relaxation processes are still not fully understood.

Different types of energy states (rotation, vibration, etc.) actually come to "equilibrium" at different times[8]. The "relaxation time" (τ) is defined as the time from the passage of the shock front until equilibrium for that type of energy state occurs. After approximately twice the mean time between collisions a Maxwellian distribution of molecular velocities will exist. This is the relaxation time for equilibrium among the translational energy states.

The rotational energy states, if any, are found to come into equilibrium with the translational states after 10 to 300 collisions per molecule, depending upon the gas. Next the vibrational states come to equilibrium with the rotational and translational states. Molecular dissociation is the limit of vibration and will reach equilibrium at approximately the same time. After a few thousand collisions the electronic excitation states come to equilibrium with the others. Ionization represents the limiting case of electronic excitation and occurs almost simultaneously.

Ionization relaxation is the longest and therefore the most easily studied for any gas. To study any relaxation time, the gas and the conditions can often be chosen to suppress or lengthen the other relaxations. For example,

rotational relaxation studies have been done using diatomic molecules in a cooled tube with weak shocks[9] so that essentially only two rotation states are excited.

During the relaxation processes the pressure will remain approximately constant but the other gas variables will adjust toward their final values. The particle number density or mass density will always increase, while the translational temperature decreases. Note that during the relaxation, "temperature" has no clear meaning since each energy type will show a different apparent temperature (or temperature cannot be defined).

5. The Problem

In 1957 Petschek and Byron[10] published the results of a study of ionization relaxation times in argon using an electron probe to measure the instantaneous density of electrons in the plasma. Their conclusions have been generally accepted since that time, but several questions concerning their treatment of results will be discussed in Chapter V. To find the activation energy for the relaxation process the logarithm of the relaxation time ($\log \tau$) was plotted versus the reciprocal of the absolute plasma temperature ($1/T$). A parallel straight line was obtained for each initial pressure, P_o, showing τ is proportional to $\exp (E_A/kT)$ as expected. All data reduced reasonably well to one line if $\log (P_o \tau)$ vs $(1/T)$ was plotted instead. This seemed reasonable since collision frequency was ex-

pected to be proportional to the pressure and τ to be inversely proportional to the collision frequency. This experiment is accepted as evidence that the ionization relaxation time is inversely proportional to the pressure, or number density.

In 1968, as part of a study of mercury vapor in a heated shock tube Y.M. Kim included a brief study of ionization relaxation[6]. He found that log ($P_o \tau$) vs (1/T) was not nearly as good a line as log τ vs (1/T). It therefore appeared that no pressure dependence of τ exists for mercury vapor--in direct contradiction to the results for argon. Recently Dunaev et al[11] have tried to account for this difference by postulating the formation of an excited diatomic mercury molecule which acts as the rate-controlling species during relaxation.

Kim's result might be questioned because it was based on only 13 points, P_o was varied less than a factor of 2, and the shocks at the small τ end of the graph were subject to relatively large error. However, the difference in pressure dependence may be due to other inherent differences in the gases or techniques. Both gases are monatomic (above room temperature) but the low ionization potential of mercury results in a very much higher final degree of ionization. Also, the massive atoms cause shocks in mercury to be much stronger than "similar shocks" in argon because shock strength depends on the Mach number not on the absolute velocity (see Chapter II).

For these reasons, it was felt that Kim's conclusion should be checked and that it was especially important to observe much weaker shocks in mercury as a better comparison with argon. That study is the main purpose of the present work. Also, more data might help in explaining this unexpected result for mercury and lead to a better understanding of the ionization relaxation process as well.

It has also been apparent for some time that minute amounts of impurities have a very major effect on the relaxation times. This was noted first by Petschek and Byron[10], but the role which impurities play is still not understood. One great advantage of the heated shock tube is the ability to bake out the tube and obtain unusually high test gas purity. Therefore, a brief study of impurity effects is included in this present work.

CHAPTER II

SHOCK CALCULATIONS

1. General Solutions

Experimental observations indicate that steady-state flows exist behind a shock front and the influence of a growing boundary layer on the thermodynamic variables of the respective flows is small within the observation region. Therefore, the shock tube flow may be treated as a one dimensional steady-state problem in a non-viscous fluid--an approximation which promises the merit of simplicity[12].

The transition from a state of low pressure and temperature to one of high pressure and temperature is governed by the conservation laws of mass, momentum, and energy across the shock front[13]. Following the recent general formulation* outlined by Kim[14]; if the primary and reflected shocks are numbered in order 1, 2, 3, etc. then for the n^{th} shock front we have,

(Mass) $$\rho_{n-1} \, v_{n-1} = \rho_n \, v_n \, , \qquad (1)$$

(Momentum) $$\rho_{n-1} \, v_{n-1}^2 + p_{n-1} = \rho_n \, v_n^2 + p_n \, , \qquad (2)$$

(Energy) $$h_{n-1} + \tfrac{1}{2} v_{n-1}^2 = h_n + \tfrac{1}{2} v_n^2 \, , \qquad (3)$$

where the subscripts n refer to variables behind the n^{th}

---

* The general formulation is no longer than that for the primary shock alone. Formulation is detailed in order to demonstrate Kim's new method completely.

shock and n-1 to variables ahead of the shock.

The specific enthalpy, h, is

$$h = e + p/\rho \,, \qquad (4)$$

and ρ, v, p and e are respectively the density, the flow velocity in the local coordinate system moving with the shock front, the hydrostatic pressure, and the specific internal energy.

The equation of state of the gas is

$$\frac{p}{\rho} = \frac{RT}{\mu} \,, \quad \text{or} \quad \frac{p}{\rho} = NkT \,, \qquad (5)$$

where N, k, T, R and μ are the specific particle number, the Boltzmann constant, the absolute temperature, and the molecular weight of the gas. Since the plasma is a mixture of different particles we use the effective molecular weight

$$\mu = \sum_i \mu_i N_i \,,$$

where μ_i is the molecular weight of the i^{th} species and N_i is its fractional abundance (by particle number).

For convenience define X_n and Y_n, the density ratio and pressure ratio across the shock front as

$$X_n = \frac{\rho_n}{\rho_{n-1}} \quad \text{and} \quad Y_n = \frac{p_n}{p_{n-1}} \,. \qquad (6)$$

Now, (6) in (1) gives $v_n = v_{n-1}/X_n \,. \qquad (7)$

(6) and (7) in (2) gives $v_{n-1}^2 \rho_{n-1}\left(1 - \frac{1}{X_n}\right) = p_{n-1}\left(Y_n - 1\right) \,,$

or,
$$v_{n-1}^2 = \frac{p_{n-1}}{\rho_{n-1}} \frac{X_n (Y_n - 1)}{(X_n - 1)} \quad . \tag{8}$$

(8) in (7) gives $v_n^2 = \frac{p_{n-1}}{\rho_{n-1}} \frac{(Y_n - 1)}{X_n (X_n - 1)}$. (9)

(8) and (9) in (3) re-arranges as

$$h_n - h_{n-1} = \frac{p_{n-1}}{\rho_{n-1}} \frac{(Y_n - 1)(X_n + 1)}{2X_n} \quad , \tag{10a}$$

or as, $$h_n - h_{n-1} = \tfrac{1}{2}(p_n - p_{n-1})\left(\frac{1}{\rho_n} + \frac{1}{\rho_{n-1}}\right) \tag{10b}$$

which is the generalized Hugoniot relation for shock processes.

The total specific internal energy will be the sum of the total translation energy ($\frac{3}{2}$ kT per particle), the rotation and vibration energies ($\frac{1}{2}$kT per particle, per degree of freedom), the electronic excitation energy, and the energy of dissociation for molecules and ionization for atoms.

Therefore, using (5) $h_n = e_n + p_n/\rho_n$ becomes

$$h_n = \frac{3p_n}{2\rho_n} + \tfrac{1}{2}\sum_i (f_R + f_V + f_E)_i \, N_i \frac{p_n}{\rho_n} + \sum_i \chi_i \alpha_i N_i N + \frac{p_n}{\rho_n}$$

where f_R, f_V and f_E are the rotation, vibration and excitation degrees of freedom for the i^{th} particle species. χ_i and α_i are the ionization or dissociation potential and the degree

of ionization or dissociation for the i^{th} species.

For simplification

$$D_n = 2\sum_i \chi_i \alpha_i N_i N$$

and $$B_n = 4 + \sum_i (f_R + f_V + f_E)_i \; N_i \quad .$$

Therefore, $$h_n = \tfrac{1}{2}\left\{(B_n + 1)\frac{p_n}{\rho_n} + D_n\right\} \quad . \tag{11}$$

Put (11) in (10a), multiply by $\frac{\rho_{n-1}}{p_{n-1}}$ and re-arrange to get

$$B_{n-1} + 1 + (D_{n-1} - D_n)\frac{\rho_{n-1}}{p_{n-1}} - (B_n + 1)\frac{p_n}{\rho_n}\frac{\rho_{n-1}}{p_{n-1}} =$$

$$\frac{(1 - Y_n)(X_n + 1)}{X_n} \quad . \tag{12}$$

Let $$K_n = B_{n-1} + (D_{n-1} - D_n)\frac{\rho_{n-1}}{p_{n-1}} \quad , \tag{13}$$

and solve for X_n to get, $$X_n = 1 + \frac{B_n Y_n}{K_n + Y_n} \tag{14}$$

which is the generalized Rankine-Hugoniot relationship expressing the density ratio in terms of the pressure ratio.

If (14) is substituted in (8) for X_n we get,

$$v_{n-1}^2 = \frac{p_{n-1}}{\rho_{n-1}} \frac{(Y_n - 1)(1 + B_n Y_n)}{(1 + B_n Y_n - K_n - Y_n)} \quad . \tag{15}$$

If we now let $$r_n = \frac{\rho_{n-1}}{p_{n-1}} v_{n-1}^2 \quad , \tag{16}$$

(15) can be re-arranged as,

$$B_n Y_n^2 + (1 - B_n)(1 + r_n)Y_n + (K_n r_n - r_n - 1) = 0$$

a quadratic equation for Y_n. Since negative Y_n has no physical meaning

$$Y_n = \frac{1}{2B_n}\left\{\left[(B_n - 1)^2 (1 + r_n)^2 + 4B_n(1 + r_n - K_n r_n)\right]^{1/2} + (B_n - 1)(1 + X_n)\right\} . \qquad (17)$$

If X_n and Y_n are known, then from (5a) $\frac{T_n}{T_{n-1}} = \frac{\Gamma_n}{\Gamma_{n-1}} \frac{Y_n}{X_n}$.

$$\rho_n = \rho_o (X_n X_{n-1} X_{n-2} \cdots X_2 X_1) ,$$

$$p_n = p_o (Y_n Y_{n-1} \cdots Y_2 Y_1) ,$$

and $$T_n = T_o \frac{\Gamma_n}{\Gamma_o} \frac{p_n}{p_o} \frac{\rho_o}{\rho_n} = R \frac{\Gamma_n p_n}{\rho_n} .$$

Now $v_{n-1}^2 = (V_n + U_{n-1})^2$, with $U_o = 0$, where V_n and U_{n-1} are respectively the shock velocity, and the gas plasma velocity, measured in the laboratory coordinate system. Therefore, to find the conditions behind the n^{th} shock front it is necessary to measure only the initial gas conditions (p_o and T_o) and all n laboratory shock front velocities, V_n. The gas conditions and U_1 may then be calculated for the primary shock (n = 1), to give the initial conditions for shock front #2 (reflected shock) from which the conditions behind that front may be obtained. This procedure is repeated for each front in order, until the n^{th} plasma conditions are known.

The initial and final conditions of the gas and the degrees of freedom affect X_n and Y_n. From (14) and (17) it can be seen that X_n and Y_n, which are often used to measure the shock strength, are actually functions of r_n. r_n is thus a good measure of shock strength.

The speed of sound, c, for a gas is given by

$$c^2 = \gamma \frac{p}{\rho} = \left\{\frac{\gamma RT}{\sigma}\right\} \quad \text{therefore,} \quad c_{n-1}^2 = \gamma \frac{p_{n-1}}{\rho_{n-1}} \qquad (18)$$

where γ is the ratio of the specific heats for the gas. Substitution of (18) in (16) shows $r_n = \gamma M_n^2$, where M_n $(= v_{n-1}/c_{n-1})$ is the shock mach velocity relative to plasma n-1.

Since c is proportional to $\sigma^{-\frac{1}{2}}$, a gas composed of heavy molecules will have a lower speed of sound, and a higher Mach number (stronger shock) for the same laboratory velocity.

2. Computations

If we know the plasma conditions ahead of the n^{th} shock and calculate the conditions behind the shock assuming $B_n = 4$ and $D_n = 0$ we get the "ideal gas" conditions. This would be the thermodynamic conditions attained either for an ideal gas*, or for the gas immediately

* In this paper, the term ideal gas denotes a gas with no internal degrees of freedom. Van der Waals forces may always be neglected for gas conditions encountered in the shock tube.

behind the shock front after relaxation of only the translational energy states. Other energy states remain unchanged and would temporarily exhibit population distributions corresponding to the original temperature. It is from these gas conditions that relaxation into the other states actually occurs. For this special case calculations become very simple, especially for the primary shock, and computations can readily be done by hand. Full computations for the final equilibrium state of the non-ideal gas will require the use of a computer.

Relaxation studies are usually limited to the primary shock region where the relaxation times are longest and where computations are somewhat simpler. For the $n = 1$ shock, we will have $B_0 \equiv 4$ and $D_0 \equiv 0$ for all reasonable initial temperatures. The use of monatomic gases simplifies both the actual processes involved in relaxation (only electronic excitation and ionization exist), and the computation of final conditions, since $f_R = f_V \equiv 0$, and D_1 involves only ionization.

The calculations for values of X_1 and Y_1 (hence p_1, ρ_1, T_1) involve the summation of each electronic partition function (Z_i) to some "cut-off" energy, and the degrees of ionization (α_i), but the cut-off energies and the Z_i, themselves depend on the unknown final gas conditions (p_1, T_1). Final conditions may be assumed in order to evaluate the α_i and Z_i for use in approximating the final

conditions. These better values are then used to improve the α_i and Z_i which will, in turn, result in even better final values. This iteration process may be repeated until the input and output values agree to within any desired limit.

Kim claims[6, 14] that this simple iteration process converges very rapidly, but in fact divergence may actually result unless the original choices of values were reasonably close to the correct values. Rapid convergence, even when the original choice is quite poor, may be easily obtained if some form of interpolation based upon previous input-output values is incorporated after each iteration cycle, to obtain even better values for use in the next cycle.

For a plasma of electrons, atoms and ions we may write the Saha equations for the first two ionizations of the atoms as

$$\frac{N_+ N_e}{N_A} = \frac{Z_+ Z_e}{Z_A} e^{-\chi_A/kT} , \qquad (19)$$

and

$$\frac{N_{++} N_e}{N_+} = \frac{Z_{++} Z_e}{Z_+} e^{-\chi_+/kT} . \qquad (20)$$

N_A, N_e, N_+ and N_{++} are the number densities per unit volume for atoms, electrons, singly and doubly ionized atoms, with Z_A, Z_e, Z_+ and Z_{++} as the corresponding partition functions. χ_A and χ_+ are the effective 1st and 2nd ionization potentials of the atom.

We now define the 1st and 2nd degrees of ionization as

$$\alpha_1 = \frac{N_+}{N_A + N_+}, \quad \text{and} \quad \alpha_2 = \frac{N_{++}}{N_+ + N_{++}}. \tag{21}$$

From which if $N_o = N_A + N_+ + N_{++}$ we have,

$$N_A = N_o(1 - \alpha_1), \quad N_+ = N_o(1 - \alpha_2)\alpha_1,$$
$$N_{++} = N_o(\alpha_1\alpha_2), \quad \text{and} \quad N_e = \alpha_1 N_o(1 + \alpha_2). \tag{22}$$

Use of* $p = NkT$ and $N = N_o(1 + \alpha_1 + \alpha_1\alpha_2)$

with (22) causes (19) and (20) to simplify as

$$\frac{(1 - \alpha_2^2)\alpha_1^2}{(1 - \alpha_1)(1 + \alpha_1 + \alpha_1\alpha_2)} = \frac{Z_e Z_+}{Z_A}\frac{kT}{p} e^{-\chi_A/kT} = f_1 \tag{23}$$

and

$$\frac{(1 + \alpha_2)\alpha_1\alpha_2}{(1 - \alpha_2)(1 + \alpha_1 + \alpha_1\alpha_2)} = \frac{Z_e Z_{++}}{Z_+}\frac{kT}{p} e^{-\chi_+/kT} = f_2. \tag{24}$$

Or,

$$\alpha_1^2(1 - \alpha_2^2 + f_1 + f_1\alpha_2) - \alpha_1\alpha_2 f_1 - f_1 = 0 \tag{25}$$

and

$$\alpha_2^2\alpha_1(1 + f_2) + (\alpha_1 + f_2)\alpha_2 - (1 + \alpha_1)f_2 = 0. \tag{26}$$

If f_1 and f_2 are known (or estimated) α_1 and α_2 may be found quickly by a simple iteration process for the positive roots of these quadratic equations.

---

* All N now refer to the particle number density per cc.

If gas mixtures are used the same method is employed but further Saha equations, and a revised N are necessary to include the atoms of the second gas. The treatment of mixtures with polyatomic gases has been given by Wilkerson[15] and was used only briefly for this research in connection with the impurity studies.

For any species in the plasma, the partition function is given by $Z = Z_T Z_R Z_V Z_E$ with the index T standing for translation, etc. The atoms and ions are identical except for charge and very small differences in mass, so only their Z_E may differ. For electrons

$$Z_T = \left(\frac{2\pi mkT}{h^2}\right)^{3/2}, \qquad Z_R = 2 \quad \text{(2 spin states)}$$

and $Z_V = 1$.

Using these values in (23) and (24) for f_1 and f_2,

$$f_1 = \left(\frac{2\pi m}{h^2}\right)^{3/2} \frac{(kT)^{5/2}}{p} \frac{Z_{E+}}{Z_{EA}} e^{-\chi_A/kT} \tag{27}$$

and

$$f_2 = \left(\frac{2\pi m}{h^2}\right)^{3/2} \frac{(kT)^{5/2}}{p} \frac{Z_{E++}}{Z_{E+}} e^{-\chi_+/kT} . \tag{28}$$

It has been seen experimentally[16] that for high pressures and charge densities atomic spectra remain normal up to a certain quantum number after which the lines merge into a

continuum with the spectral series limits depressed as though a lower ionization potential existed.

Thus
$$Z_{Ei} = \sum_{E_n=0}^{\chi_i} g_n \, e^{-E_n/kT} \quad , \tag{29}$$

where g_n, E_n, and χ_i are the statistical weights, the excitation energies and the effective (lowered) ionization energy for the atom or ion considered. All g_n, E_n and the free space ionization potentials for computation were obtained from the tables by Charlotte Moore[17].

Inglis and Teller[18] took Stark broadening as the important mechanism for level spreading and found the cut-off quantum number (or χ_i) by equating the energy difference of neighboring levels to the spread of the corresponding levels. Better results take the charge screening of the plasma into account as well[19,20]. The Debye-Hűckel formula for the lowering of the ionization potential (eq. 30) is obtained this way but is valid only when the number of electrons per Debye sphere is less than one. For higher density plasmas the result of Ecker and Kroll[21] should be used.

For the present work the Debye-Hűckel cut-off is satisfactory. Thus,

$$\Delta\chi_z = \frac{e^2}{R_D}(z+1) \tag{30}$$

with
$$R_D = \left\{ \frac{kT}{4\pi e^2 \left(N_e + \sum_i z^2 N_i\right)} \right\}^{1/2} \quad , \tag{31}$$

where $z = 0,1,2$ etc for neutral atoms, 1st ions, 2nd ions, etc.

The actual $\Delta\chi_z$ used here is relatively unimportant, but some consistent cut-off procedure is necessary otherwise all Z_i are infinite. Tests show that even for relatively strong shocks tripling $\Delta\chi_z$ causes less than 1% variation in the final thermodynamic variables calculated.

If the final p, T are known, or assumed, the $\Delta\chi_z$ may be obtained from (31) for each species. These values allow the effective χ_i to be found for use in (27), (28) and (29). f_1 and f_2 can then be found for use in (25) and (26) where α_1 and α_2 are found by iteration. The shock equations (14) and (17) may then be solved to find better values for the final p, ρ and T which in turn are used (with interpolation) to begin the next cycle of iteration.

CHAPTER III

CONSTRUCTION OF THE SHOCK TUBE

1. Introduction

A heated shock tube has been in full operation at the University of Michigan since 1967. Designed and built by Y.W. Kim, its initial application was the study of high electron density mercury plasmas. Preliminary observations and construction were reported earlier[6,22].

During early work by Kim, some minor design difficulties were noted, and this chapter describes these problems and recent engineering improvements to correct them. Some suggestions for future heated tubes are included. A more complete description, which includes details for a new flush valve, and the construction for large (7") observation windows, may be found in reference 23. Fig. 2 shows the entire shock tube schematically.

The main advantages of a heated tube are the high purity levels of the shocked gas, resulting from the continual baking, and the ability to work with substances evaporable only at moderate temperatures.

2. The Expansion Tube.

The main shock tube with connected fittings and hardware, was constructed of stainless steel (Type 304). The expansion tube, including the test section, is 107 $\frac{1}{2}$" long and consists of five sections, made from seamless rectangular tubing

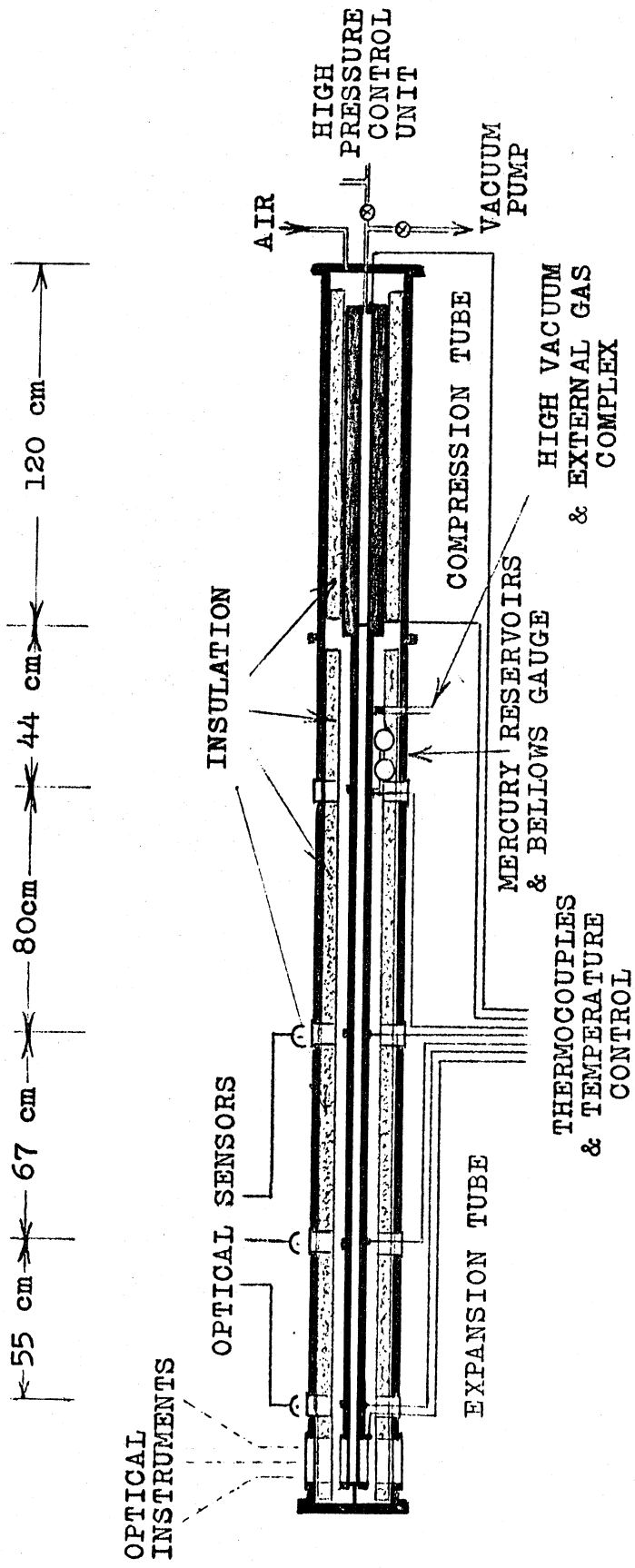

Figure 2. Schematic Drawing of the Heated Shock Tube

with 3/8" wall, inner dimensions 1.510" x 2.560", and inner corner radius 0.300".

In order to reduce boundary layer effects, the inner surface of the entire expansion tube was highly polished. Tube sectioning was considered necessary because the rectangular cross-section is extremely difficult to polish in long sections. The sections were put together by flanges 7/8" thick, and 6" in diameter. Between each pair of adjoining sections, goes a 6" diameter, 1-3/4" thick disc, containing two viewing or probe-mounting ports fitted for 2-3/4" Conflat flanges. Details may be seen in Figs. 3 and 4. The matching faces of the disc and adjoining flange have gasket grooves similar to those of the 6" Varian Conflat flanges[24].

OFHC copper gaskets, 0.080" thick, are sealed between the matching conflat grooves using ten 3/8"-24 x 4" bolts, with the flanges tightened so they come into direct face-to-face contact. Aligning is done by means of preset dowel pins, and the sections are not interchangable. All nuts and bolts are lubricated with Sauereisen graphite paste (No. 51), to prevent them from fusing together at the high temperatures.

Kim found that after a period of use any change in tube temperature caused a small vacuum leak at one of the many flanges. This could often be corrected by further bolt tightening on the correct flange[25]. Normally, neither of these should happen, according to Wheeler and Coulder[24],

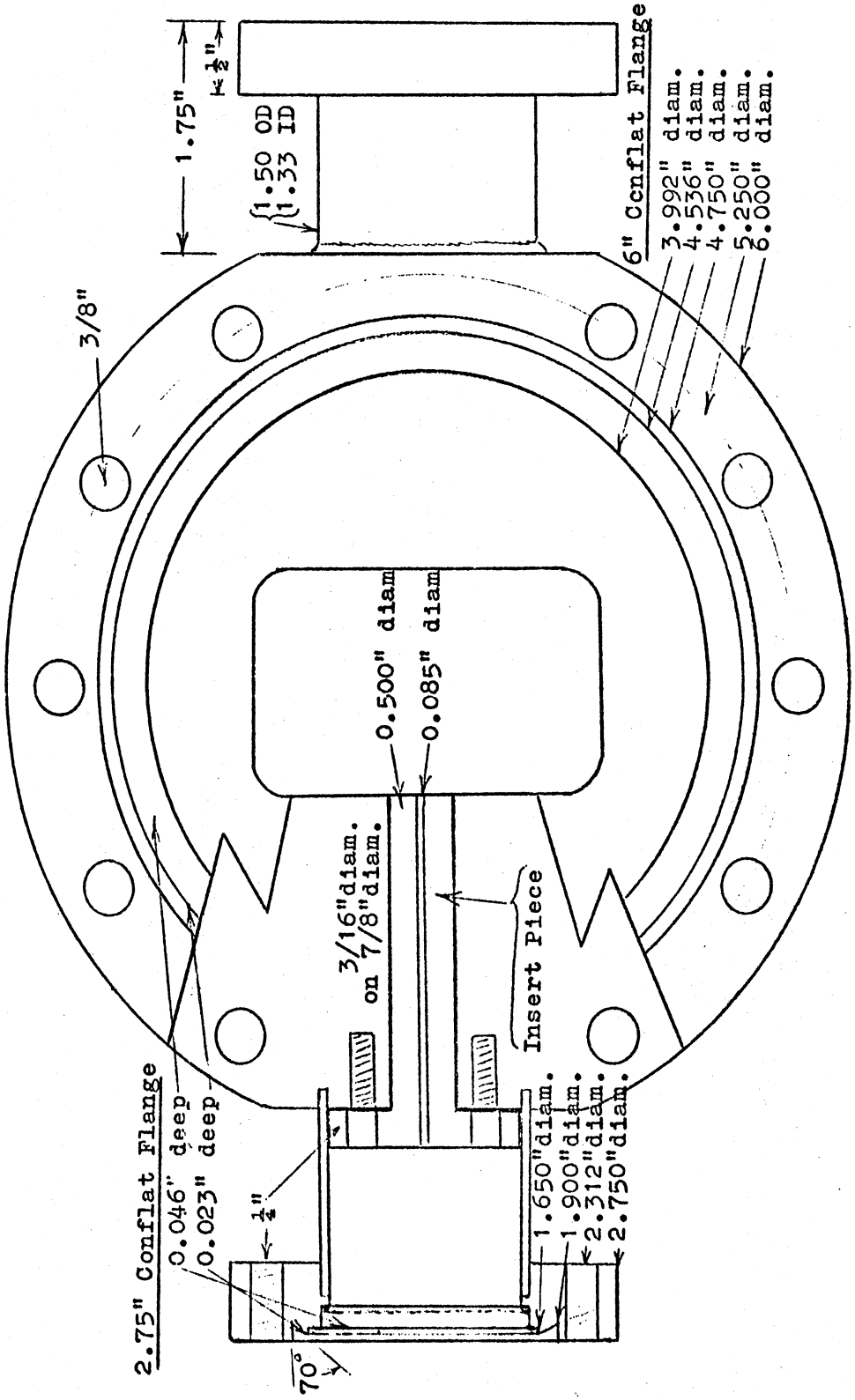

Figure 3. Partial Cutaway View of Disc Piece

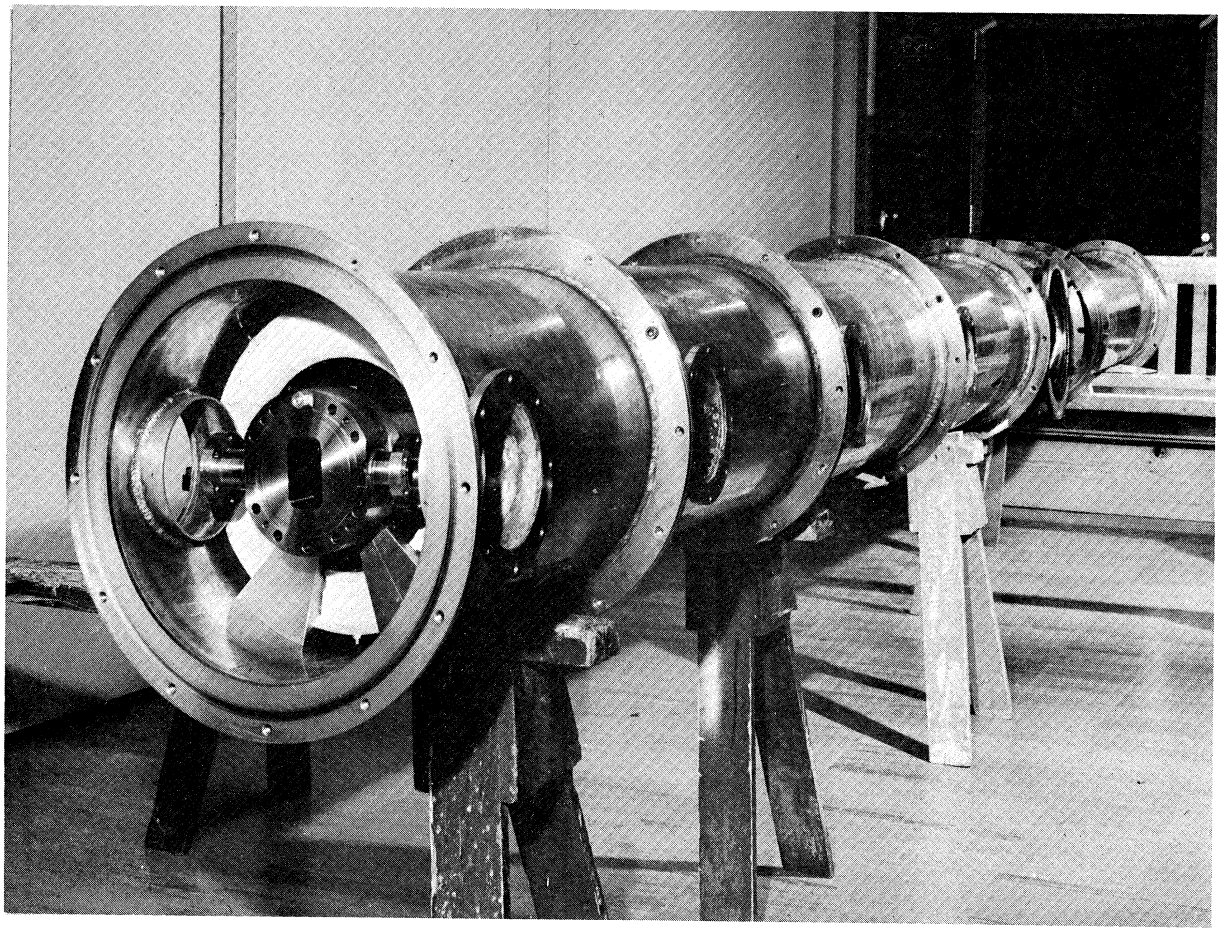

Figure 4. Partially Assembled Heated Shock Tube

who researched the Conflat type flange extensively. However, their paper did suggest several necessary modifications. First, the Conflat seal is due to the interaction of the outer circumference and the knife-edge only, and the inner part of the gasket should be free from any compression or restriction. Second, the nickel plating, which was used to protect the gasket from the mercury vapor, may chip or crack at the knife-edge, thus causing leaks. Third, the knife-edge should cut into the gasket 0.015" on each side for best results. When the tube was dismantled it was found that the knife-edges had been badly blunted by the harder plated gaskets. These three faults were corrected by re-machining all flanges, and eliminating gasket plating. Overhauls will now be necessary about every two years since the unplated gaskets are more rapidly attacked by the heated mercury vapor.

A fourth problem, which probably aggravated the effect of the other three, and vice versa, was the asymmetric cooling of the flanges. This has definitely been noted[24] to cause leaks. The expansion tube was originally supported by a pair of short, large cross-section legs at each flange (see Fig. 4). To correct this heat loss problem, the legs were removed, and the tube suspended from the outer casing by four pairs of 6" long, 1/4" stainless steel eye bolts, fastened to the smaller observation port flanges on the discs. In designing a new tube this suspension would be best, but with the eye bolts attached to special brackets welded to

the tube between flanges. With such a suspension an extra 1/4" diameter, 6" bolt, between the end of the test section and the outer casing, was necessary to prevent tube recoil.

Also, since each disc requires 6 seals which must be maintained, (2 large and 2 small Conflat, and 2 windows) it would be worth the effort to polish the tube in longer pieces. It is also worth considering the use of a circular shock tube, which can be cheaply and easily honed as one piece, but flow studies would then be difficult to interpret. To cut heat losses, machining, and leaks, the discs should be eliminated completely and the observation ports mounted directly on the tube wall using a structure similar to that described for the newest test section.

3. The Compression Tube

The compression section is constructed as a single piece 48" long, of the same rectangular tubing. Flanges 1" thick are welded on each end between the tubing and a surrounding steel tube, 6" in diameter and 1/4" thick, and the space between filled with Sauereisen, low expansion, high temperature cement (No. 7).

The compression tube is connected to the expansion tube by six sets of 5/8"-10 x 4", heat-treated nuts and bolts. A round, soft metal diaphragm is squeezed between the faces of matching flanges. Two concentric knife-edges on each flange complete the vacuum - high pressure packing. The total seal proved good from 5×10^{-5} mm. Hg. to 3000 psi.

For replacing the diaphragm after each shot, the compression tube rolls on two pairs of Fafner ball-bearing casters mounted on a slotted angle rail structure in a section of the outer casing.

4. Heating

Although it performed adequately, Kim's original cylindrical oven[6] occasionally developed electrical shorts causing the wire winding to burn out. Also, its weight and bulk were a severe handicap during maintenance and overhaul. These faults were overcome with a new heating structure which also allows much more rapid heating and cooling of the shock tube, and requires only one-tenth the power consumption. (100 watts per foot at 500°C).

The simple shock tube sections are wrapped with 4" wide asbestos tape, then #16 Chromel "C" heater wire is wound over this, and the structure covered by Sauereisen electric heater cement (No. 63). The test section and the mercury reservoir area, being more complicated shapes, are heated by means of "Hot-Foil" heating tapes. The current to each section is controlled individually by variac to give uniform tube temperature, checked by thermocouples. Since the temperature of the tube, once established, was very stable no special automatic temperature control was needed.

The Chromel wire is far heavier than necessary for the steady state currents used even at 500°C, thus allowing current increase for rapid heating during temperature changes

without wire burn-out. The cement and asbestos serve as electrical insulation from the tube. The cement also protects the asbestos from air since its binding material deteriorates at very high temperature, and in the future, if necessary, will hold the decomposed asbestos and the wire in place.

Two layers of $1\frac{1}{2}$" thick fiberglas pipe covering (7" and 11" inner diameters) were fitted around the shock tube inside the outer casing. Joints were staggered to prevent air convection to the outer casing as much as possible. The highest temperature usable is determined by the deterioration of this insulation and should be in excess of 500°C. More insulation is present on the outside of the casing. The entire area inside the casing is not filled by insulation because the uniformity of the tube temperature depends on free air convection near the tube.

Iron-constantan thermocouples were attached at 6 points on the tube. The test section, the reservoirs, the 4 disc pieces and each end of the compression tube are monitored points. The thermocouples are resistance matched, and using a multipole switch are checked individually by connecting the desired thermocouple to a 0 - 260°C API Pyrometer (Model 603-1). Temperature can be controlled to within $\frac{1}{2}$°C.

5. The Outer Casing

The outer casing is also divided into sections, with lengths roughly matching those of the shock tube, and made of half-hard temper brass tubing with a 14" inner diameter

and 3/16" thickness. The sections are joined by firebox quality steel flanges. Wrapped around each tubing is 1½" fiberglas insulation covered with 4" wide asbestos tape making the overall diameter almost 18". Each section has two side openings of 5-1/4" diameter, allowing access to the shock tube at the viewing port positions. One 12" diameter opening at the middle section accommodates all the vacuum components to the main tube and mechanical feed-throughs to the mercury reservoirs.

The failure of an observation window or of other packings of the shock tube may cause exposure of laboratory personnel to the extremely hazardous mercury vapor. The present safety system depends upon the casing being moderately air-tight. The inside of the casing is connected, at the test section end, to a long ½" diameter pipe opening directly outdoors. This prohibits any gas build-up inside the casing which would cause leaks into the laboratory. When working with poisonous vapors the outer casing is never opened after firing a shock until the high pressure is released, and an attempt is made to evacuate the shock tube. If a good vacuum is not obtained, then the casing is flushed with compressed air to drive any remaining vapors from the casing.

With the new improvements the brass casing now serves no useful purpose, in fact it is a handicap during any repair or overhaul. A new "casing" is suggested for future tubes, which is cheaply and easily constructed. The shock

tube is suspended by longer eye bolts to a metal frame, but with extra bars fastened near the diaphragm flanges to prevent recoil motion. Three layers of fiberglas pipe covering surround the tube (7", 10" 13"), with joins staggered, and wrapped with 4" wide asbestos tape. This "casing" is lined with aluminum foil as a vapor barrier, either inside or between the layers of pipe covering, and suspended from the metal frame. Electrical and instrumental access may be obtained directly through the insulation without causing appreciable leaks.

Optical clearance for a small observation port is easily obtained through a thin-walled steel tube which is in contact with the port at one end and passes through the layers of insulation to the outside. This viewing system is actually used with the new test section. A light weight window frame can easily be fitted into the insulation to clear an area for larger test section windows. The new heating, thermocouple, and safety systems are still applicable. The insulation casing for the compression section may be fitted tightly to the tube and the entire section suspended from a carriage which rolls back and forth on the metal frame.

6. The New Test Section

All window seals of the heated shock tube must be highly vacuum and pressure tight. The heating requirements and the presence of mercury specify the use of stainless steel O-rings and soft metal gaskets. These are adequate for metal-

to-metal seals, but for optical windows metal O-rings tend to chip the surface, and fusing metal into optically flat glass is not easy. Instead, direct contact between the glass and metal O-ring is avoided by using a thin layer of Kapton polymide film, called H-film. The H-film is available in 0.001" to 0.010" thicknesses, and has proved highly satisfactory.

H-film is extremely strong and retains its strength over a temperature range far greater than used here. Because H-film does not "flow" extensively under pressure the best seal is made by pressing an area only about 1/16" wide, about the area under a stressed metal O-ring. Broader areas require increased bolt loads, and often cause window cracking due to increased stresses.

Vacuum seals for large windows are extremely difficult to achieve and maintain at high temperatures. After moderate success with attempts to improve Kim's original large (7") window test section, it was decided that the remaining faults[23] could only be corrected by building a costly new 7" test section. Instead, a very simple structure was tried which proved to be excellent, and solved all the window problems.

The new test section, shown in Fig. 5, consists of a regular piece of the shock tube with 3 observation ports, or windows, 2.750" apart (at 20°C) along each side, and the final window 1.75" from the end-wall. Windows on opposite sides are exactly aligned so that beams of light may be

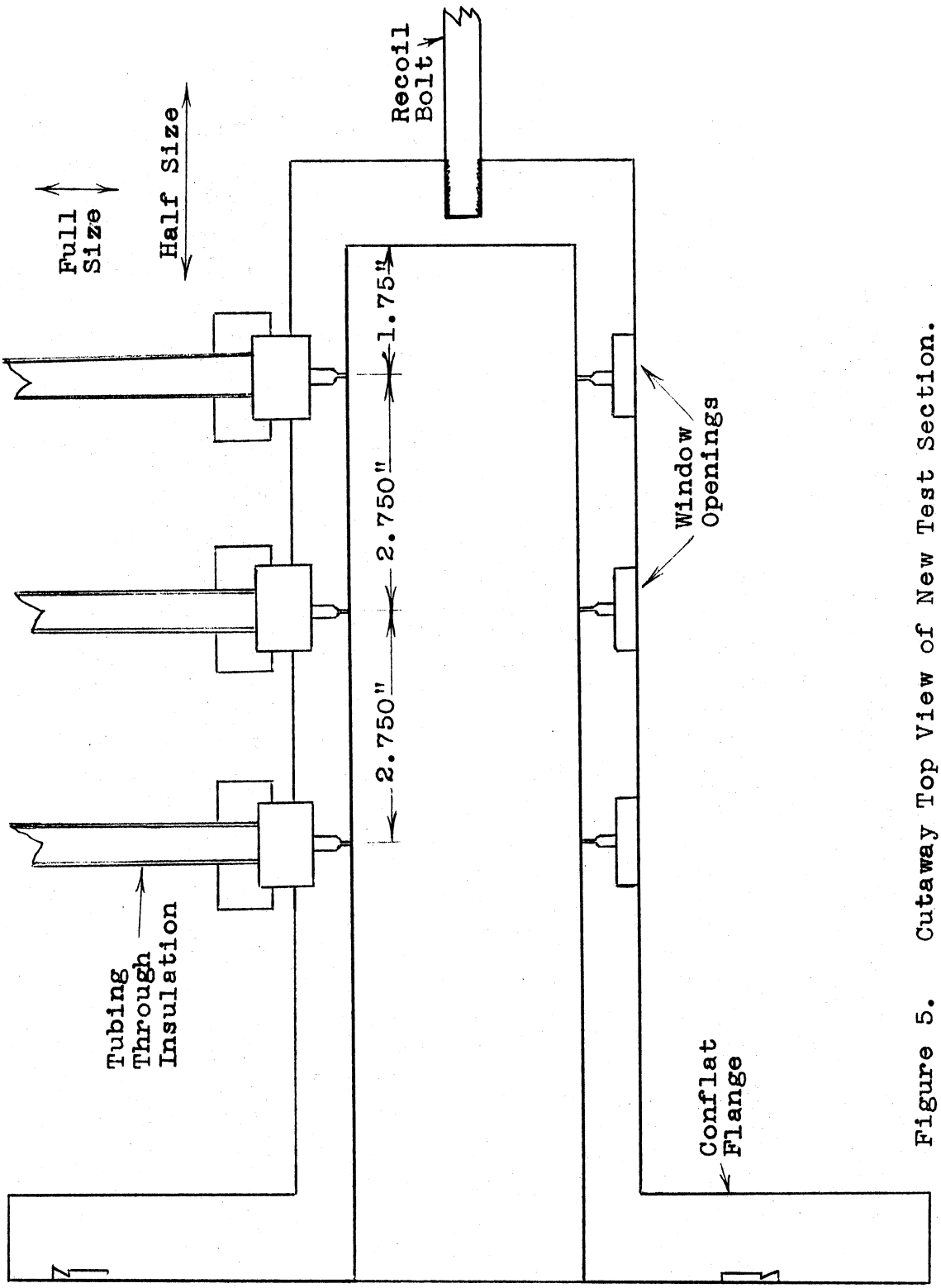

Figure 5. Cutaway Top View of New Test Section.

passed through the tube perpendicular to the tube axis. Details of the window structure are shown in Fig. 6.

A vertical arrangement of 3 holes is used in each window to allow more light to be collected. Holes are used, instead of a narrow vertical slit, for minimum gas flow disruption. The windows are set into the wall, and the hole size stepped, to keep reflections from hole walls to a minimum. The raised sealing ring allows all pressure to be limited to a 1/16" wide area on the H-film, and removes pressures from the edge of the glass. O-rings are not used because they are difficult to change after use, and the O-ring groove would weaken the tube wall.

The glass windows, 3/8" thick and 1" in diameter, may be replaced by quartz or other material, if desired.

7. The Mercury System

A special gauge, and a mercury reservoir are installed within the oven, close to the shock tube. This system must be kept at the same temperature as the tube, or higher, since the maximum vapor pressure usable will be that of the coolest part of the entire system. The gauge and reservoir are separated from one another, and connected to the tube using two bakable valves made with stainless steel bellows and O-rings. The arrangement is shown in Fig. 7.

The common difficulties encountered in measuring pressures of heated vapors are the condensation at cold spots caused by connecting a gauge at room temperature, and the

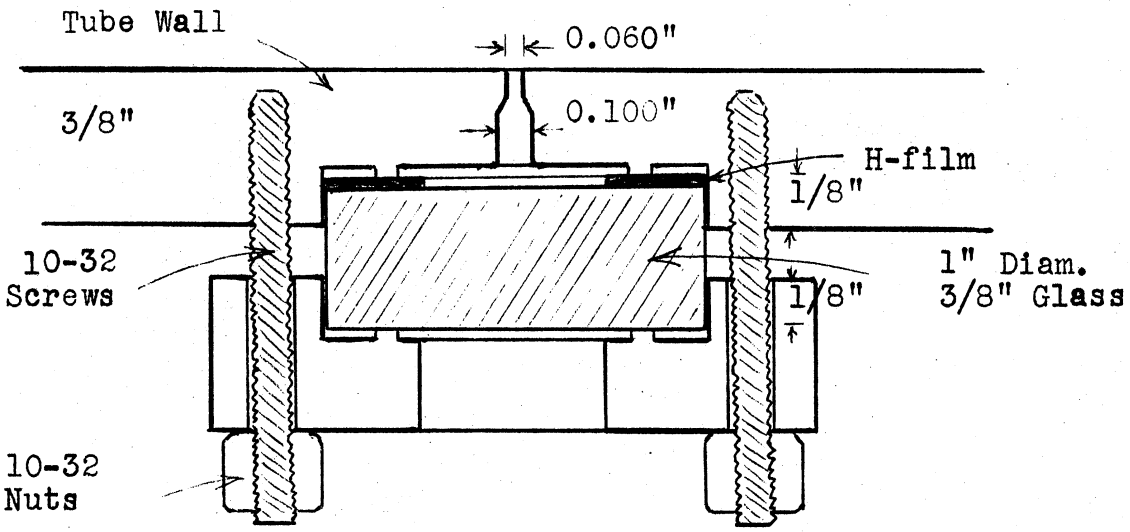

A. Top Cutaway View (Double Actual Size)

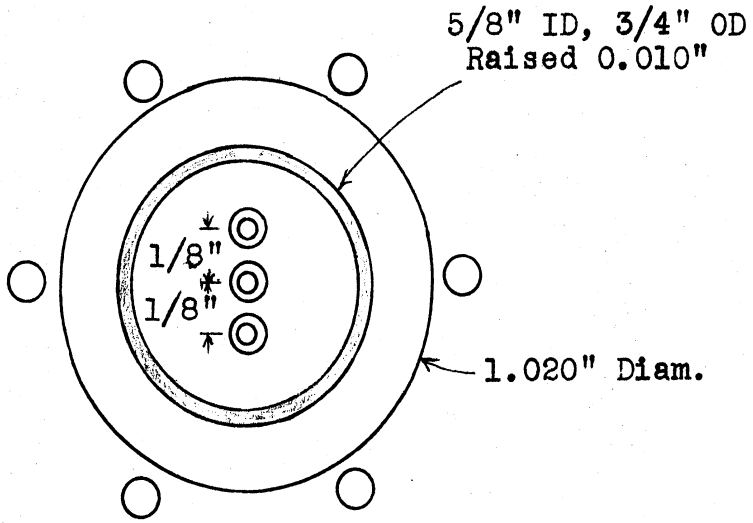

B. Front View of Tube Wall (Double Actual Size)

Figure 6. New Test Section Window Structure.

failure of many molecular gauges when excessively heated. As a result, Y.W. Kim designed a gauge, shown in Fig. 7 which can operate at the tube temperature.

The space enclosed by a stainless steel sylphon bellows (spring rate 17.9 lb/in. at 20°C.) is filled with the gas to be measured and the bellows are housed in a small vacuum cylinder so that the pressure outside the bellows may be independently regulated. This method eliminates calibration which would be necessary if the bellows expansion were used as the pressure scale--the spring rate varies with temperature. The effect of cooling and of the temperature gradient on the pressure distribution in the outer system are negligible.

An insulated electrode is sealed into the outer cylinder and extends far enough to make contact with the top of the bellows when both sides are fully evacuated. A microammeter is used to measure the contact current. Before any gas measurement, the air pressure outside of the bellows is raised until the electrode contact is nearly broken, at say 30 μAmp. The air pressure is then measured by an oil manometer and used as a zero point. The air pressure is then raised by the desired mercury gas pressure (meter reads zero now), and the mercury gas is then filled into the bellows (and shock tube) from the liquid reservoir until the gauge contact is restored. The outside air pressure is then carefully adjusted until the meter again reads 30 μ amp. The final manometer reading corrected by the zero point value gives the mercury

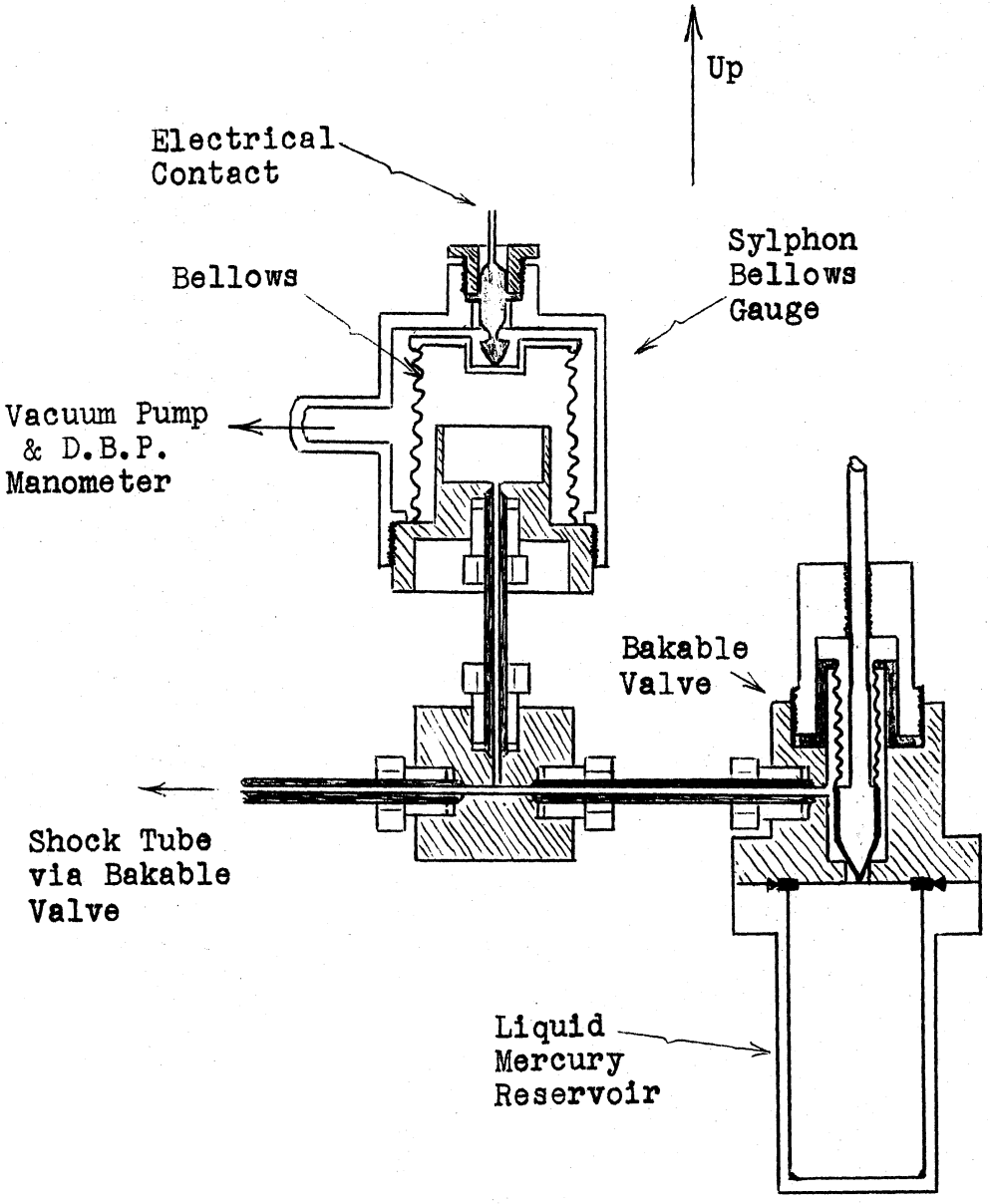

Figure 7. Bellows Gauge and Mercury Reservoir.

gas pressure.

This filling and measuring procedure allows accurate determination of the pressure (but not an exact pre-determined value) while keeping impurity contamination to a minimum. The liquid mercury in the reservoir was thoroughly outgased before use to guanantee purity, but tube leaks and outgasing are always present. Experimental shocks were never fired when the total tube leak (plus outgasing) was greater than 0.2 μ/minute, which gives a maximum of 0.6 μ impurity in the 3 minutes necessary to close and fill the tube before firing the shock. For the lowest values of P_o used (10 Torr) this 0.6 μ represents an impurity of 60 parts per million.

Maintenance of this bellows gauge is simple and the stainless steel sylphon bellows have very long life. The present bellows has been in use since construction 3 years ago. However, the electrical contact within the gauge sometimes becomes bad, and requires opening the gauge to polish the surfaces involved.

8. Gas Handling Systems

A Duo-Seal pump (Type 1 402-B) backs a CVC metal mercury diffusion pump (Type MHG-180) to evacuate the tube and the gas-vacuum complex. A CVC glass trap between the pumps guards against mercury contamination. The diffusion pump is connected to a manifold through a stainless steel water cooled trap, and the bakable flush valve connects the manifold to the shock tube and closes the tube off completely

from the vacuum system when a shot is fired. Also connected to the manifold are an Autovac gauge (Type 3294-B), and an oil manometer, which are employed for monitoring the various pressures.

Within one minute the expansion section is evacuated to 1 μ Hg and ten minutes pumping brings the tube pressure to 0.001 μ Hg, with a leak rate of about 0.1 μ/minute. Brief exposure of the tube to air has no significant effect on the pumping rate, however, an hour is required to bring the tube back to uniform temperature after the outer casing is opened for a diaphragm change.

Typical gases used to drive shocks are hydrogen, helium and nitrogen. These are commercially available in bottles at pressures up to 3500 psi. These bottles are connected, via stainless steel flexible hoses, to the compression section, and a manifold, which allows the various gases to be used separately, or as mixtures.

CHAPTER IV

OBSERVATION TECHNIQUES

1. The Schlieren System

The arrangement for the schlieren system at each window of the test section is shown schematically in Figure 8. A 34 watt tungsten filament lamp (G.E. type BXJ) illuminates a 0.010" wide slit, S1 as the source for 3 schlieren systems. Lens L1 with slit S1 at the focus results in a parallel beam of light. Two sets of adjustable mirrors separate this beam into 3 parts and align each of these parallel beams through a different test section window. The emerging beam passes through lens L2 and forms an image of S1 at the knife-edge position, the focus of L2. The moveable knife-edge is adjusted over the image of S1 so that very little light normally reaches S2, a 0.006" wide slit in front of the photomultiplier tube.

A density gradient anywhere within the parallel section of the beam will deflect part of the beam and change the amount of light reaching S2. Density gradients in the shock tube may thus be detected, while a new constant density in the tube will cause no change in the schlieren light signal. Best results are obtained if the test section is imaged at S2 with unit magnification. (distances = 2f). This is a compromise between spatial resolution and light intensity at the photomultiplier. The knife-edge is positioned so that the increase in density as the primary shock passes will

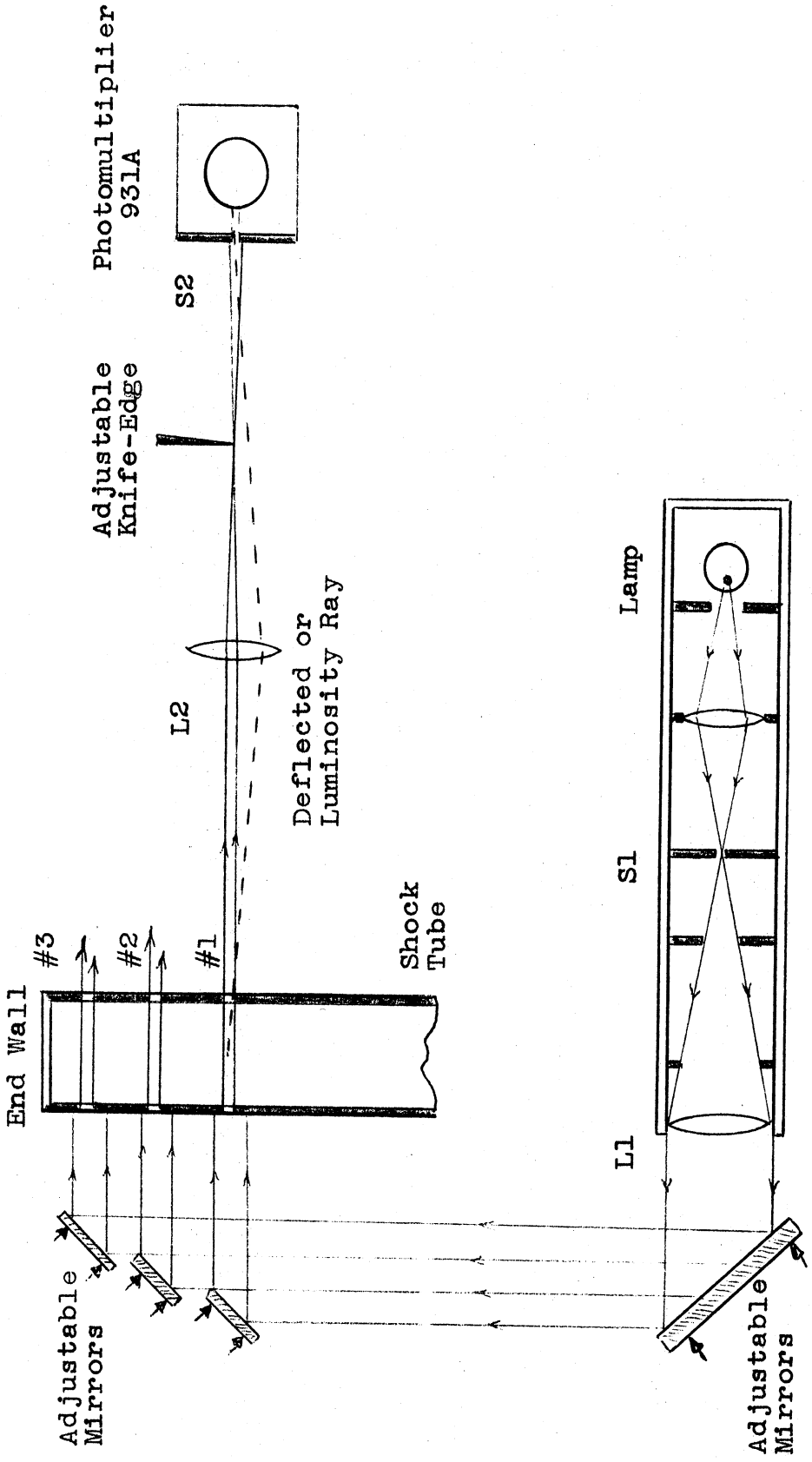

Figure 8 . Schematic Drawing of the Schlieren System

cause an increase in the light reaching S2. Note that small adjustments of the knife-edge, which is on the axis of the optical system, greatly affect the amount of luminosity observed at S2.

As the shock front passes the window, the gradient is so steep and short that light passes very strongly for only a fraction of a microsecond. A fairly insensitive schlieren system is used in order that only the large density gradient at the shock front can be seen. A measure of the sensitivity of a schlieren system is given by[26] $\frac{\Delta I}{I} = \frac{\alpha f_2}{d_2}$, where f_2 = focal length of the lens L2, d_2 = the width of the S1 image at the knife-edge, and α = the angle which the light beam is refracted. This equation is valid only for gradients which do not move the S1 image entirely off the knife-edge.

The shock front velocity is determined from the time between the schlieren pulses from different windows and the inter-window distances.

2. Luminosity Observation

Because the test section is focussed on S2 the photomultiplier will automatically record the plasma luminosity as well as the light from the schlieren system. The photomultiplier does not record all the plasma radiation because the glass windows and tube envelope absorb ultraviolet with wavelength shorter than 3200A°, and the 931A tube is not sensitive to wavelengths longer than 6500A°.

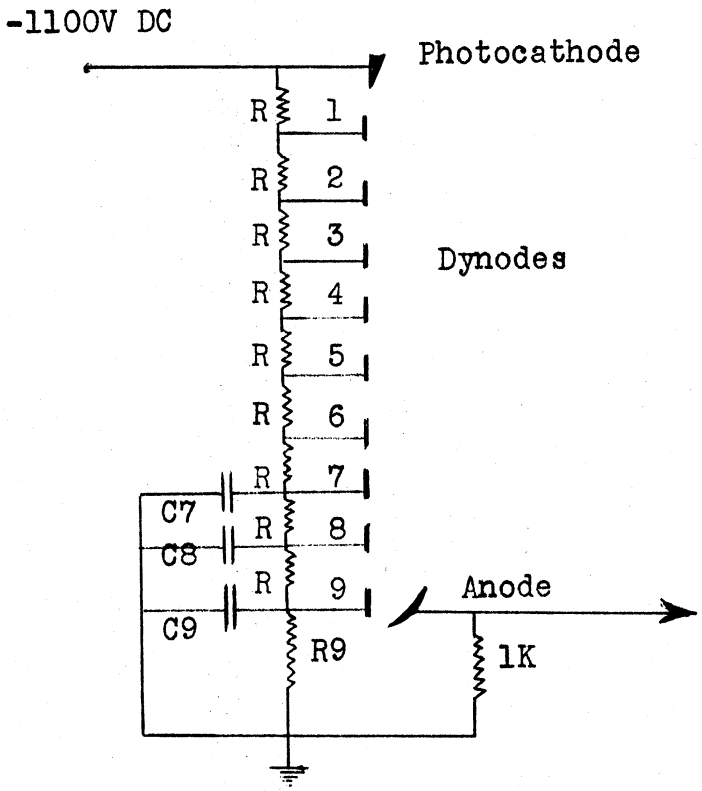

	R	R9	C9	C8	C7
Tube #1 :	37K	49K	4.0μf	0.5μf	0.05μf
#2 & #3 :	100K	120K	0.001	0	0

Figure 9. Schematic of the Photomultiplier Circuits

The circuits for the photomultiplier tubes are shown schematically in Fig. 9. The circuit for tube #1 (re shock passage) is designed mainly for observing the plasma luminosity without distortion. The #2 and #3 tubes are used only for shock speed timing and their outputs are limited to 1 volt for pulses longer than 5 μsec. duration. The output of tube #1 is free from distortion up to 30 volts for signals from 0.1 μsec. to 0.01 sec. Output limiting and distortion are controlled by the choice of resistances and capacitances, and the values used are shown with Figure 8.

A Tektronix Model 551 dual beam oscilloscope was used to record results. The output of photomultiplier #1 (schlieren plus luminosity) was displayed on the lower beam, while the outputs of #2 and #3 were added by the oscilloscope pre-amplifier (type CA) and shown inverted on the upper beam. Sweep was triggered (internally) by the schlieren pulse on #1.

The sweep speed was chosen to give accuracy in determining the shock velocity. The gain on the upper beam pattern must be kept small to ensure that the pattern is not lost off-scale. This is the main reason for limiting #2 and #3 tube outputs to 1 volt each. Observations are virtually useless if the shock speed is not known (and hence the gas conditions).

For accurate determination of the relaxation time τ, it is desirable to have the #1 pattern large, so that changes in slope are readily apparent, and to have τ occupy

a large fraction of the 10 cm trace. The output of tube #1 was also observed using a Tektronix Type 535A oscilloscope with the sweep and gain set to give a good relaxation profile trace.

The oscilloscope patterns are recorded on type 47 Polaroid film, and a "zero" trace recorded as well for reference. Contact prints of typical oscilloscope patterns for mercury are shown below.

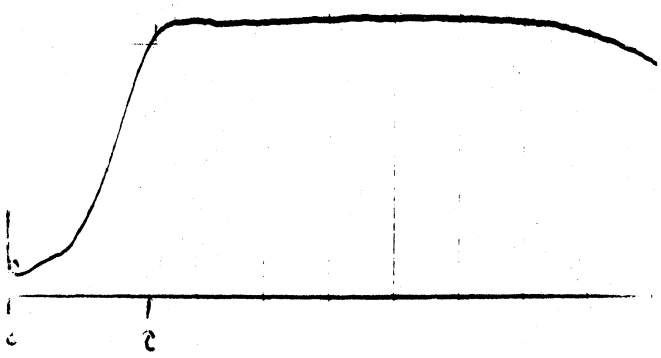

M-41*

Oscilloscope 535A

Sweep = 5 μs/cm

p_o = 29.1 Torr

T_o = 514.2 °K

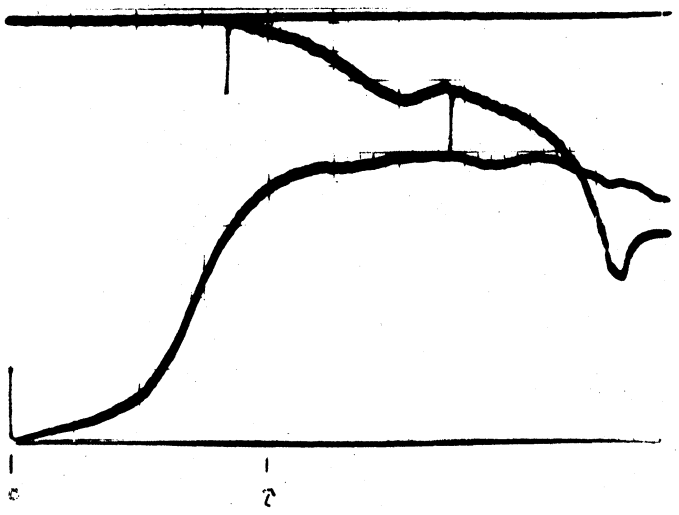

M-10

Oscilloscope 551

Sweep = 20 us/cm

p_o = 16.1 Torr

T_o = 513.2 °K

* M denotes shocks in mercury, A shocks in argon.

3. Limits on Observations

The two pictures below were obtained for the same weak shock in argon. Neutral density filters are used to cut the luminosity suitably. No schlieren light or knife-edge is present so triggering occurred for the first oscilloscope when the luminosity became large enough, and the second was triggered simultaneously by the first.

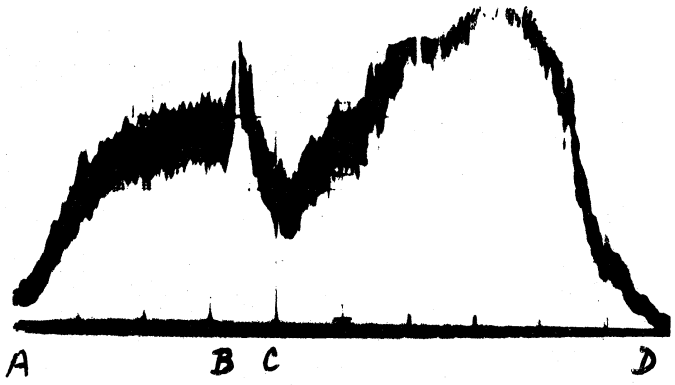

10% of light from window #1

Sweep = 20 μs/cm

Gain = 0.5 v/cm

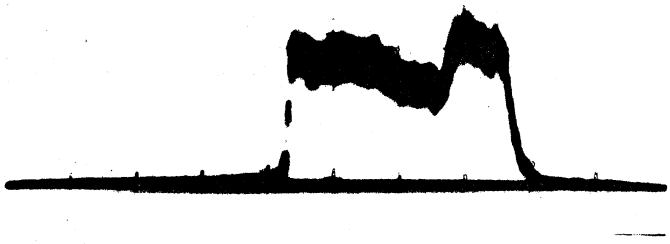

0.01% of light at window #2

Sweep = 20 μs/cm

Gain = 0.5 v/cm

These pictures show examples of some problems encountered with the present observation technique. In the first picture, the section A to B is similar to the luminosity curve of M-41. τ is very long and relaxation appears to be just complete when the interface arrives at 70 μsec. (B).

Longer τ could not be observed. Instead of the luminosity dropping abruptly when the interface arrives, a spike appears with the interface. (B→C). The spike is probably due to extra luminosity caused by impurities in the commercial grade driver gas in the region where the driver and test gases diffuse together. When the shock luminosity is greater this spike vanishes by comparison.

The large hump (from C to D) is due to scattered light from the very bright plasma behind the reflected (n = 2) shock. This light grows as the reflected slug lengthens and approaches window #1, then decreases again as the interface causes the slug to decrease in size. The maximum light here is only about 0.003 of that actually seen in the reflected shock plasma (second picture). As shock strength is increased the size of the hump (due to reflected shock luminosity) decreases relative to the maximum primary luminosity, but the hump is always present.

For stronger shocks, τ is shorter, but the larger shock velocities cause the hump to occur much earlier, even before the interface passes. This hump on top of the flat primary luminosity curve eventually makes it impossible to be sure that relaxation is complete, and the shock strength range to be studied is effectively limited. Treating the test section walls to cut the reflections would help, but treatment with molten sodium dichromate, for example, has been observed to cause boundary layer problems[25]. A better solution would be a greater separation of the end-

wall and window #1 so that the scattered light from the reflected shock will be reduced considerably, and occur much later.

The second picture shows the reflected (n = 2) shock at window #2 (at 85 μsec.), with the intensity reduced by neutral density filters. The filtering has cut the primary luminosity and tube light reflections to insignificant values ($X10^{-4}$). Note that there is also an n = 3 shock (at 135 μsec.), apparently reflected from the interface just ahead of window #2, since the interface passes at 150 μsec. Both of these shocks show radiation decay (luminosity decrease with time).

For mercury, the luminosity of very strong shocks became so large that observations with the basic system could not be made. The luminosity was reduced by neutral density filters so the photomultiplier was not overdriven but this reduced the schlieren light at the same time. When the schlieren light is reduced too far, the pulse cannot be seen and the oscilloscopes do not trigger at "zero" time. This problem was overcome, however, by using a laser* as the schlieren light source for this part of the work. The laser is extremely bright, which allows a greater luminosity range to be studied with the aid of neutral density filters. Color filters may also be introduced to cut the mercury

* Spectra Physics model 132 helium-neon gas laser of 1 milliwatt with $\lambda = 6328$ A°

luminosity without affecting the size of the schlieren pulse. The schlieren pulse size varies with p_o, which prohibits the study of very low p_o shocks--unless the more sensitive laser schlieren system is used.

4. Relaxation Times

The laboratory relaxation time (τ_L) is not the relaxation time (τ) which the gas actually experiences. In fact, the time scale of the entire luminosity profile is distorted because we observe gas flowing past a fixed position, instead of moving with the gas and observing the relaxation. Zero time for the laboratory time scale is determined by the passage of the shock. At laboratory time $t_L = \ell/V$, (32) where V is the shock velocity, the shock will be ℓ cm beyond the window. The gas which is then at the window was actually shocked t seconds earlier, and has receded from the shock at a relative velocity of V-U, where U is the gas flow velocity. Therefore, the particle time corresponding to t_L above is

$$t = \ell/(V-U). \qquad (33)$$

Eliminating ℓ between (32) and (33) gives

$$t = Vt_L/(V-U). \qquad (34)$$

Using Eq. 1 from Ch. II, we can write the relation between the laboratory and particle times for any point in the relaxation as

$$t = (\rho_1/\rho_o)t_L , \qquad (35)$$

and, $$\tau = X_1\tau_L .$$

Note that this derivation assumes that U (or ρ_i) remains constant during relaxation--this is only approximately true. The laboratory time scale is not only incorrect by a multiplicative factor, but is actually somewhat distorted due to the variations of ρ_i (or U).

The laboratory relaxation time will be the time between the schlieren pulse and the onset of constant luminosity, however, determination of the exact time at which constant luminosity begins is usually quite difficult. All oscilloscope traces show some electronic noise and random fluctuations, and near maximum luminosity the relaxation curve approaches its final height somewhat asymptotically (see M-10 Sec. IV-2). If the final approach is truly asymptotic then theoretically all relaxation times are infinite--in practice, relaxation is complete when the difference between the luminosity and the final asymptotic height is less than the average plasma (and noise) fluctuation.

In the present research, the laboratory relaxation time is taken to be the time from the schlieren pulse until the luminosity is within 5% of its final asymptotic value. The final height can be determined easily and quite accurately for all pictures. With this particular choice for τ_L we are not usually within the average plasma and noise fluctuation level but do include almost all of the relaxation curve in our measurement. Values for τ_L , which are ob-

tained in this manner, are quite consistent when a picture is measured several times by different persons.

5. Errors and Corrections

The oscilloscope sweeps were calibrated using a 1 MHz crystal oscillator. At the same time a correction was established for the non-linearity of each oscilloscope sweep. All sweep corrections were quite small ($< 1\%$), but were applied to all data collected.

The use of three windows allows shock velocity determination from windows #1 to #2, and from #2 to #3, to measure the shock deceleration. No deceleration was noted for any argon shock but all mercury shocks showed some, with deceleration becoming greater as the shock strength increased. The effect was never more than 2%, and a linear correction was applied to all mercury shocks in order to find the shock velocity at the position of window #1. Calculations allowed for the thermal expansion of the tube.

A traveling microscope permitted measurement of the pictures to better than $\pm$ 0.01 mm. With such measuring accuracy the shock speeds were determined to within $\pm$ 0.05%. The tube temperature was determined to better than $\pm$ 0.1%. The greatest error results from the initial pressure values which could only be measured slightly better than $\pm$ 1% (for p_o = 10 Torr--the greatest error).

Errors in the laboratory variables (U, P_o , T_o) result in errors in all calculated thermodynamic variables for the

final gas conditions (P_1, T_1, etc). Test computations show that in the present research all calculated pressures, mass densities, and particle number densities will be within $\pm$ 2% of the correct values (error due mainly to Δp_o). Final temperatures are in doubt by $\pm$ 3/4% (due to errors in T_o and U). The values for electron number density (N_e), electron pressure (P_e), and the degree of ionization (α_1) are the most sensitive to changes in the initial values, but will still be correct to within $\pm$ 4%.

Laboratory values for the relaxation times can always be determined within $\pm$ 3%, with most within $\pm$ 2%-- the accuracy depending upon the smoothness and size of the luminosity profile.

CHAPTER V

EXPERIMENTAL RESULTS

A. Mercury

1. Introduction

The data from the present study have been reduced, and the results are displayed in a series of graphs. The original laboratory data (P_c, T_o, V, τ_L) are tabulated in the Appendix. The shocks observed cover a range of Mach numbers from 4.7 to 10, and P_o from 10.7 Torr to 41.5 Torr. Final plasma temperatures range from 4035 °K to 9626 °K, with α, the final degree of ionization between 1.1×10^{-5} and 0.12. The particle relaxation times observed are from 10.8 μsec. to 548 μsec.

It is common practice[6,10] to assume that the relaxation process will obey a relationship similar to many chemical reactions, that is

$$\tau = A \exp(E_A/T), \qquad (36)$$

where E_A is the "activation" or characteristic energy for the process (in °K), and A may be a function of any (or all) of the plasma thermodynamic variables. If the plot of $\log(G\tau)$ against T^{-1}, where G is some function of the thermodynamic variables, shows less point scatter than the plot of $\log \tau$ against T^{-1}, then τ must be a function of G. Therefore,

$$\tau = B/G \exp(E/T), \qquad (37)$$

where B is a slower varying function of the plasma variables than A. If G includes all of the functional relationships, then B will be a constant, and the graph $\log(G\tau)$ against

T^{-1} will show only experimental scatter. The slope of the graph x 2.303 will be E_A in degrees Kelvin.

In order to more clearly demonstrate the expected dependence of τ on P_o, the graphs presented distinguish shocks on the basis of their P_o values (high, medium, low). The curves for the graphs are drawn by eye to represent the best fit to the experimental points. Slope variation limits are determined by the most extreme curves which can be drawn consistent with the data points. All starred variables (eg. T^*) refer to the "ideal" plasma conditions, that is, the conditions immediately behind the shock after relaxation of only the translational states. Unstarred variables (eg. T) refer to the final (relaxed) plasma conditions. All "ideal" and final variables are computed as indicated in Chapter II.

2. Pressure Dependence of τ

Figures 10 and 11 correspond to the graphs of Petschek and Byron[10] for argon. Figure 10 is the plot of log τ against $1/T^*$. The plot shows a tendency for points to form a pattern sloping up to the right (low T^*) but the scatter of points is very extensive (100-200%). However, from the identification of data points by their P_o value, it is apparent that high P_o points all fall low in the plot pattern, while low P_o points are all high in the pattern.

Figure 11 is the plot of log $P_o\tau$ against $1/T^*$. This plot shows considerably less scatter (now 50-70%) than

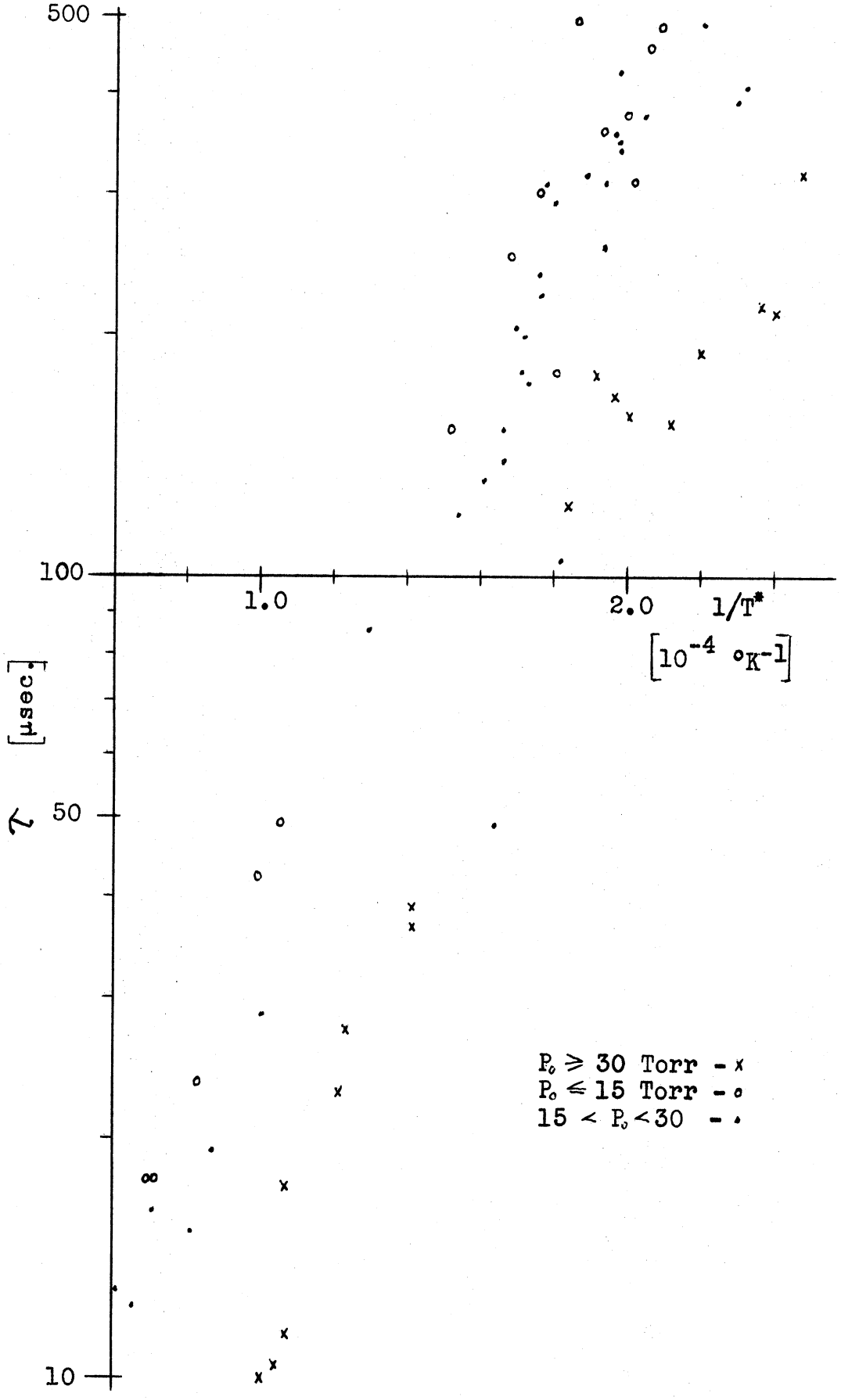

Figure 10. Plot of log τ against 1/T* for Mercury

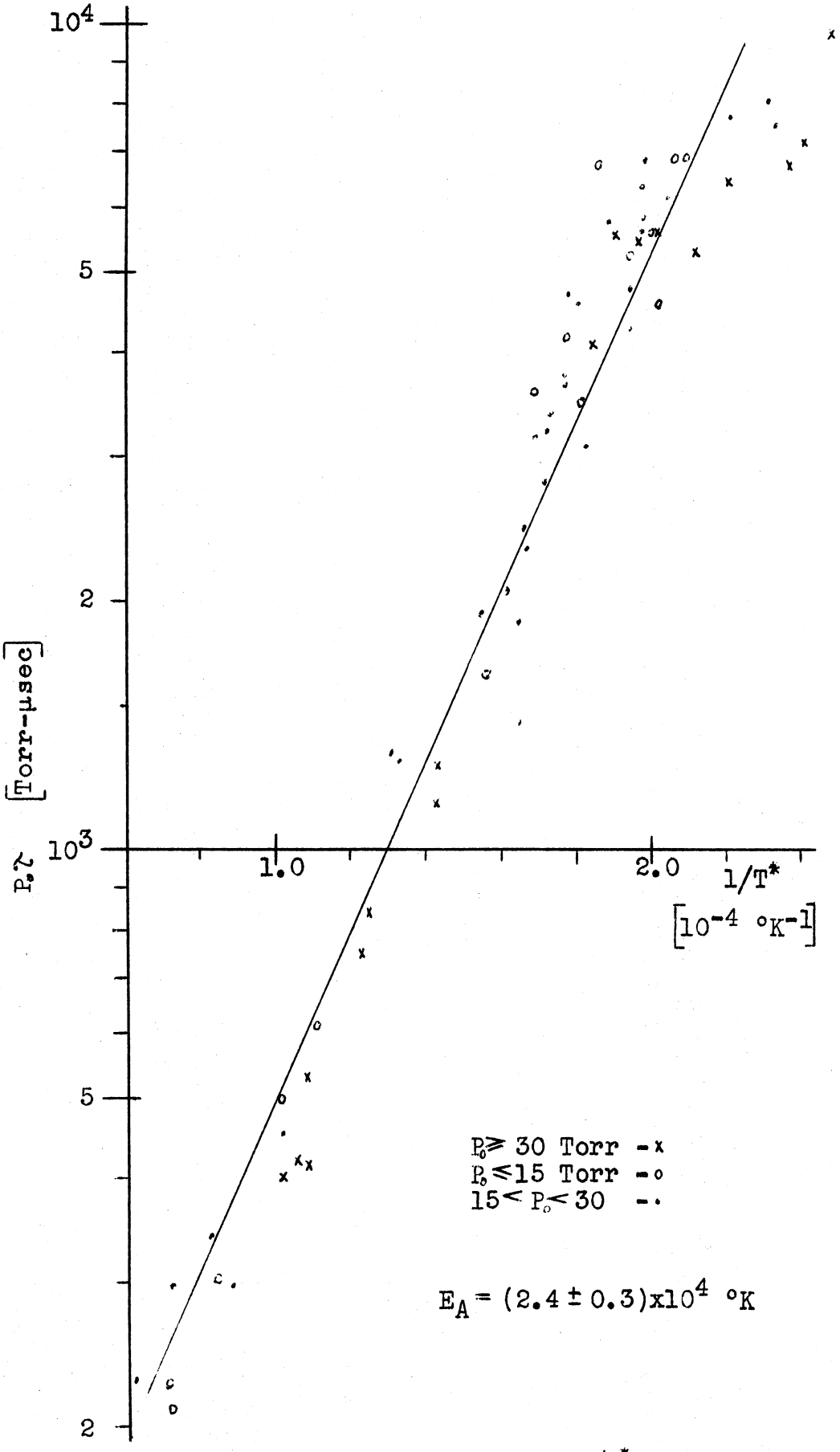

Figure 11. Plot of log $P_o\tau$ against $1/T^*$ for Mercury.

Figure 10, with points representing different P_o values fairly well intermingled along a line with positive slope. The remaining point scatter is still far greater than that due to experimental errors (see Sec. IV-5) but the scatter has been reduced significantly by the introduction of P_o. We can therefore conclude that mercury shows the same dependence on initial pressure as other monatomic gases--data are consistent with $\tau = BP_o^n \exp(E_A/T)$, where B is independent of P_o, only when n is approximately -1. This is a direct contradiction of Kim's result[6].

At first it may seem surprising that τ depends upon P_o, the pressure in the tube before the shock arrives. For the same T_o and T^*, P_o is proportional to N^*, the ideal atom number density behind the shock. Therefore, Figure 11 actually shows that τ depends on N^*, and some researchers[27] prefer to refer to this as a density dependence.

3. Temperature Dependence of τ

For the same energy, electrons are approximately 10^5 times as effective as mercury atoms in causing ionization during a collision, therefore when the degree of ionization (α) becomes greater than 10^{-5} the remaining relaxation process will be dominated by electron-atom collisions. Petschek and Byron[10] were the first to divide the total relaxation time into stages during which different processes govern the relaxation. They were also the first to point out that the electron temperature must be considerably below

the atom temperature during relaxation.

Different temperatures for atoms and electrons in the same gas are possible because the two components are well insulated from one another energetically. The fraction of a heavy atom's energy which is transferred to an electron in a collision is roughly equal to the mass ratio of the particles. For the electron-mercury atom collisions this is approximately 10^{-6}. Since the average atom thermal energy is $\sim$1 eV, or about one-tenth of the ionization potential, 10^{-7} of the energy required to create a new electron is transferred to the electrons in each collision. Therefore, 10^{7} collisions are necessary for each new electron produced, but only one or two collisions between electrons will cause a Maxwellian distribution. The electrons will therefore be in Maxwellian distribution at all times, with the high energy tail of the distribution continually losing energy as ions are created.

Harwell and Jahn[28] later showed experimentally that for argon, xenon, or krypton, the early stage of ionizational relaxation was due mainly to atom-atom collisions. Atom-atom collisions first create excited atoms, then further collisions of the excited atoms result in ionization. Ionization is controlled by the production rate of the excited atoms. Many people have attempted, with limited success, to describe the relaxation process mainly in terms of these two types of collision processes. The most complete mathematical treatment is that of Wong and Bershader[29], who

also calculate the electron temperature (T_e), relative to the atom temperature (T_A) at all times during relaxation. From their work, and the experiments of Morgan and Morrison[30], we know that the electron temperature is approximately equal (but slightly lower) to the final plasma temperature (T) throughout relaxation.

For relaxations where the final degree of ionization is high (as in the present research), the electron-atom collision process will be dominant throughout much of the relaxation time. Therefore $T_e (\doteq T)$, and not T^* should be the relevant temperature for the relaxation. The use of T^* would only be correct for studies of the initial ionization rates[28,30], or where only the atom-atom collision process occurs.

Figure 12 is the plot of log τ vs T^{-1} which shows essentially the same features as Figure 10. Comparing Figures 10 and 12 it can be seen that the use of T rather than T^* causes the pressure dependence to appear less significant at the lower (high T) end of the graph--even though the range of P is greatest here. Figure 13 is the plot of log $P_o\tau$ vs T^{-1} which shows a fairly good line with positive slope over most of the range but with more scatter and indication of a bend (towards the horizontal) at the low T end of the plot. Figure 13 shows significantly less scatter than the corresponding Figure 11 especially at the high temperature end of the graph.

From the comparison of Figures 10 and 11 with Figures 12 and 13 we can conclude that the final plasma temperature

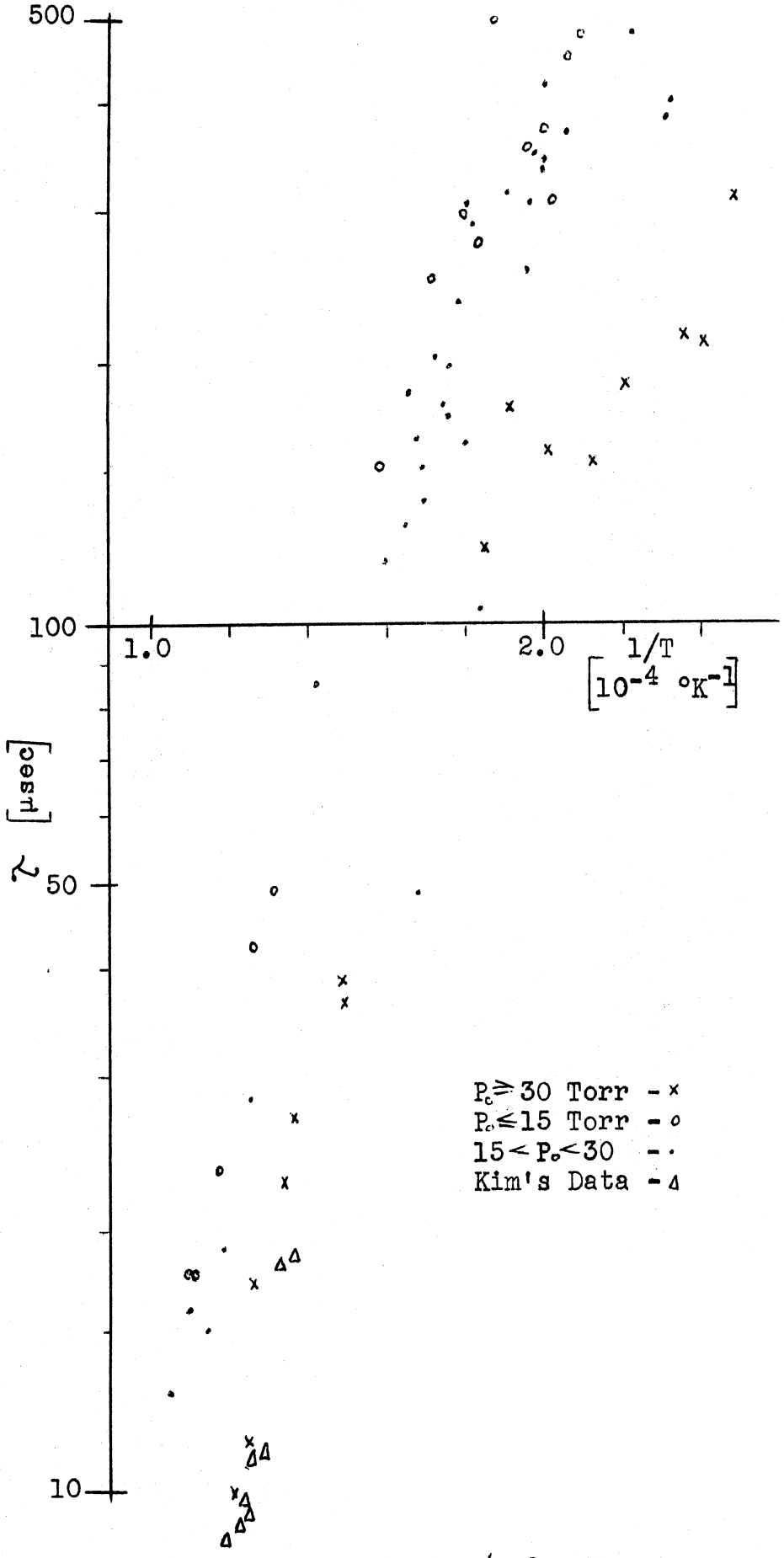

Figure 12. Plot of log against 1/T for Mercury.

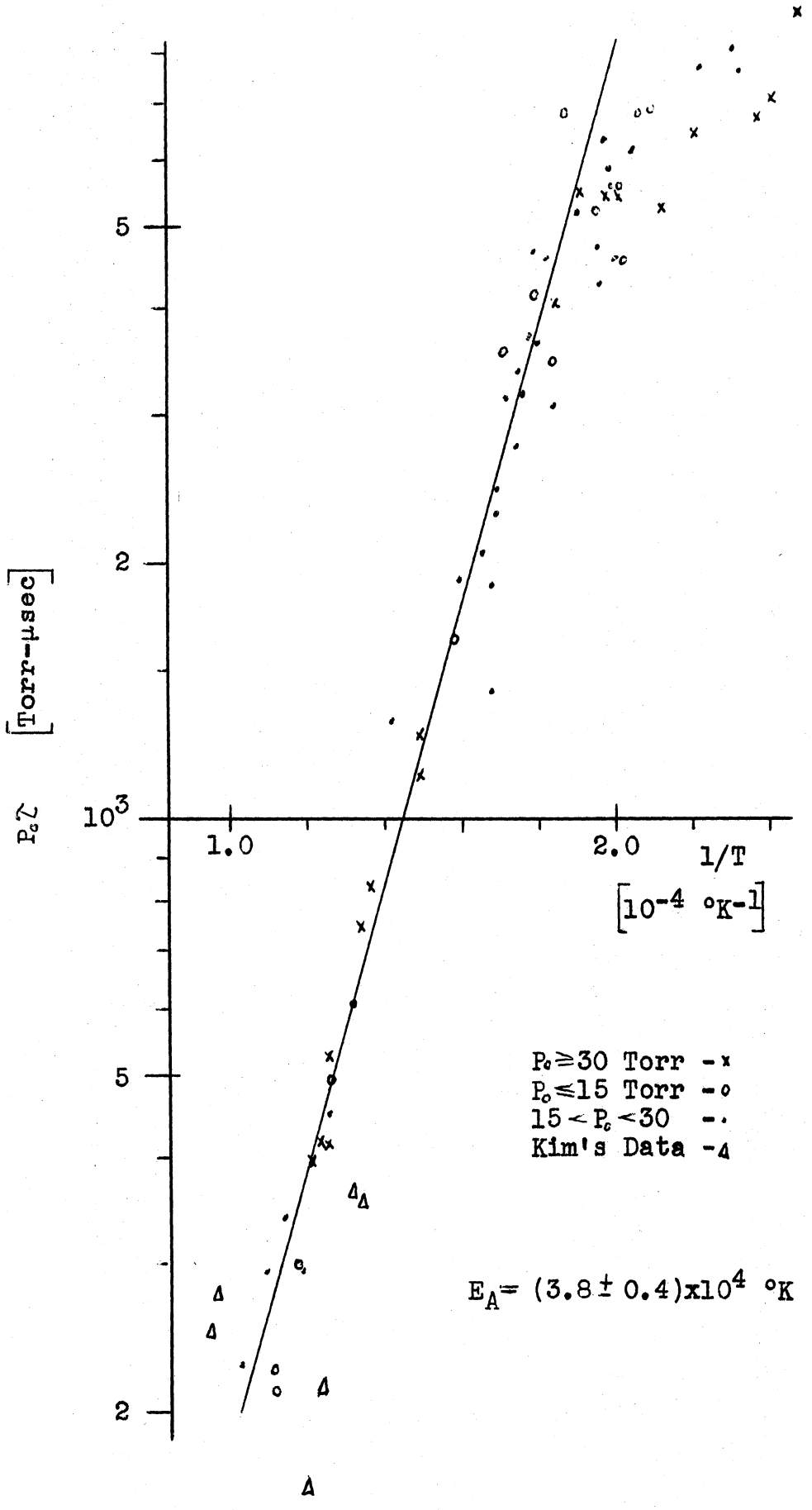

Figure 13. Plot of log $P_o\tau$ against 1/T for Mercury.

(or T_e) is a more significant temperature than T^* for the total relaxation time in a highly ionized plasma.

4. Radiation Decay

Both Figures 11 and 13 seem to show an over-correction for pressure in the lowest part of the graph (low P_o values are below the medium P_o values). This is probably due to the strong radiation decay which is present behind the high temperature shocks. Shocks typical of this high temperature region are shown in Figure 14. The attainment of equilibrium is taken to be the highest point of the trace, although the form of the curve suggests that if radiation decay were not present, the luminosity might have risen higher than this value. Therefore, the measured values for τ_i at high temperatures may be too short--the error increasing as the effect of the radiation decay increases with temperature. Pictures from shocks M54 and M55 show the increase of radiation decay with final temperature. Shock M66, at a higher temperature, actually shows a decay between the other two shocks. It would appear that, for the same final temperature, radiation decay is more important for lower pressures. This is probably due to the increased optical thickness (especially to resonance radiation) of the higher pressure gas. We might thus expect that the measured τ_i for low P_o (high T) points in Figures 11 and 13 are decreased more than the higher P_o (high T) points.

This radiation effect would also tend to account for the

M54

P_o = 12.33 Torr

T = 7636 ^oK

Sweep = 5 μs/cm

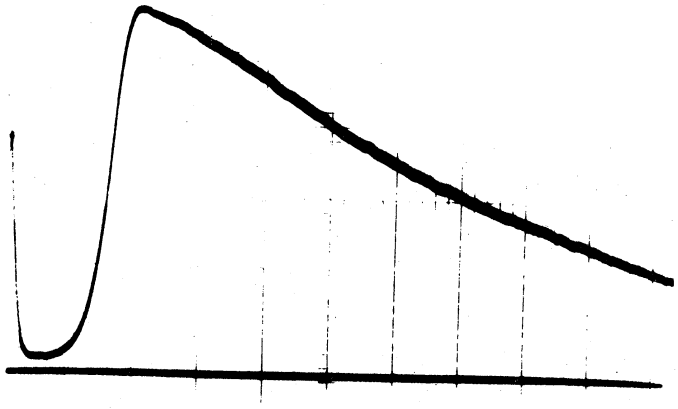

M55

P_o = 11.71 Torr

T = 7948 ^oK

Sweep = 5 μs/cm

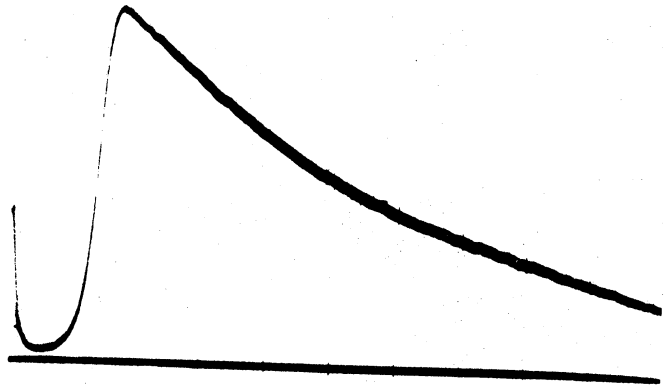

M66

P_o = 41.46 Torr

T = 8252 ^oK

Sweep = 5 μs/cm

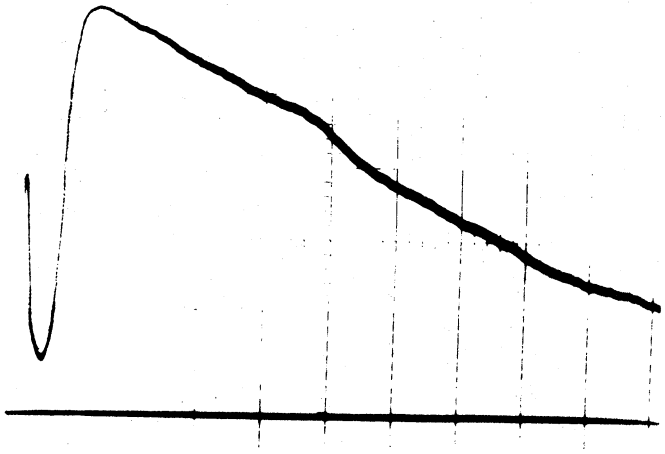

Figure 14. Pictures of Radiation Decay in Mercury.

apparent lack of pressure dependence which Kim observed. All of his shocks fall in the very high temperature and low P_o region where the effect is greatest (8000-10,000 °K and 10-20 Torr).

5. Dependence of τ on Electron Number Density

The comparison of the relaxation process with chemical reactions which resulted in Eq. 37 was quite superficial and should be re-examined. For the type of chemical reaction which most nearly resembles the collision-ionization process Fowler and Guggenheim[31] show that the reaction rate constant (number of reactions per cc per sec.) is,

$$k = C^{-1} \exp(-E_A/T) , \qquad (38)$$

where E_A is the activation energy, and C may be a function of the chemical concentrations and/or the temperature (the plasma variables in our case).

In the present reaction $k = dN_e'/dt$, where N_e' is the electron number density (or atomic ion density) at any instant. We may therefore re-write Eq. 38 and integrate over the relaxation process to give,

$$\int_0^{\tau} dt = \int_0^{N_e} C \exp(E_A/T) dN_e' , \qquad (39)$$

where N_e is the final electron number density in the plasma. Eq. 39 can be integrated to give,

$$\tau = CN_e \exp(E_A/T), \qquad (40)$$

if T and C remain constant throughout the relaxation--which

is approximately true[29,30] (from before T_e = T final). From Eq. 40 we would expect τ to be a function of N_e.

Figure 15 is the plot of $\log(\tau/N_e)$ against T^{-1}. In Figure 15 the pressure dependence is quite apparent. The plot separates distinctly into points grouped on the basis of their P_o values, with high P_o shocks always lowest. The point scatter may have been reduced by N_e (re Fig. 12), but this is not immediately apparent because of the different graph scale used.

Figure 16 is the plot of $\log(N^*\tau/N_e)$ against T^{-1}. This graph shows an excellent grouping of points, independent of their P_o values, along a curve with positive slope. The curve appears to be a straight line which bends toward the horizontal at lower temperatures. A careful comparison of Figures 13 and 16 shows that the introduction of N_e has reduced the point scatter very slightly (by ~10%) especially at the low T end of the graphs. We may thus conclude that τ does depend upon the electron number density. Since electron-atom collisions play a major role in the present relaxations it is not surprising to find that τ depends on both N^* and N .

Figure 17, $\log(N^*\tau/N_e)$ against (T^*), is plotted for comparison with Figure 16, to demonstrate that with the N_e dependence of τ included, the use of T rather than T^* still results in less scatter.

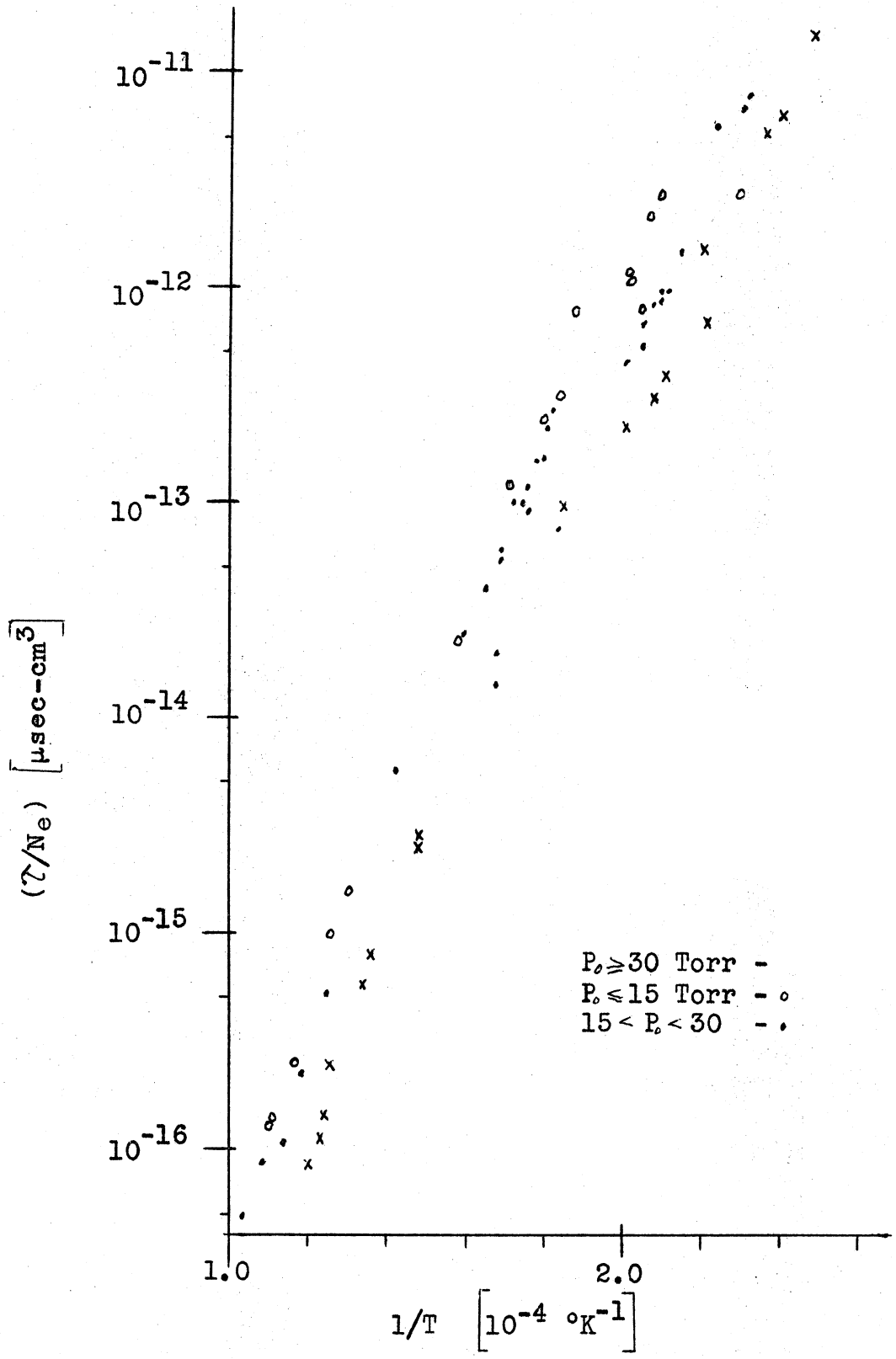

Figure 15. Plot of log(τ/Ne) against 1/T for Mercury.

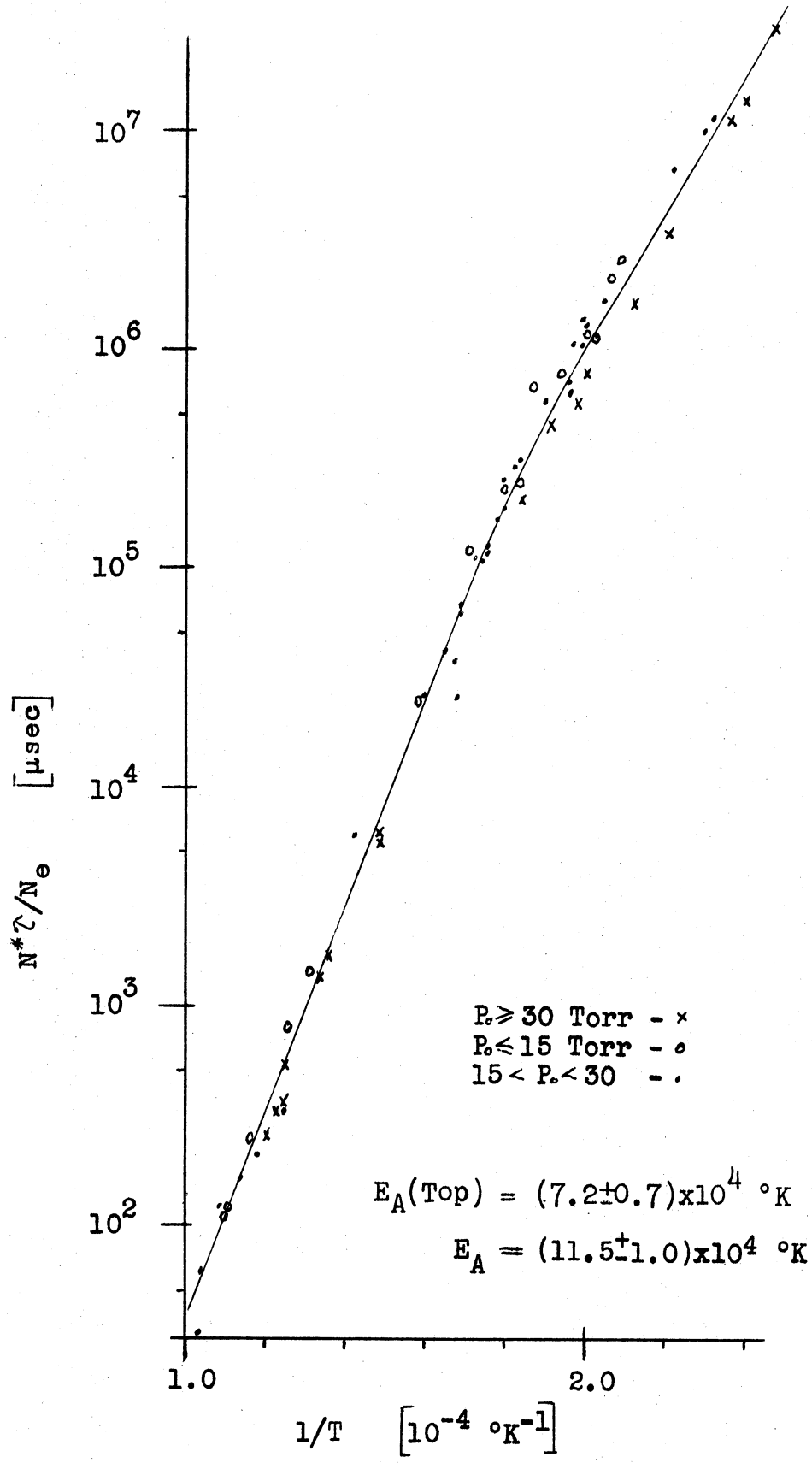

Figure 16. Plot of $\log(N^*\tau/N_e)$ against 1/T for Mercury.

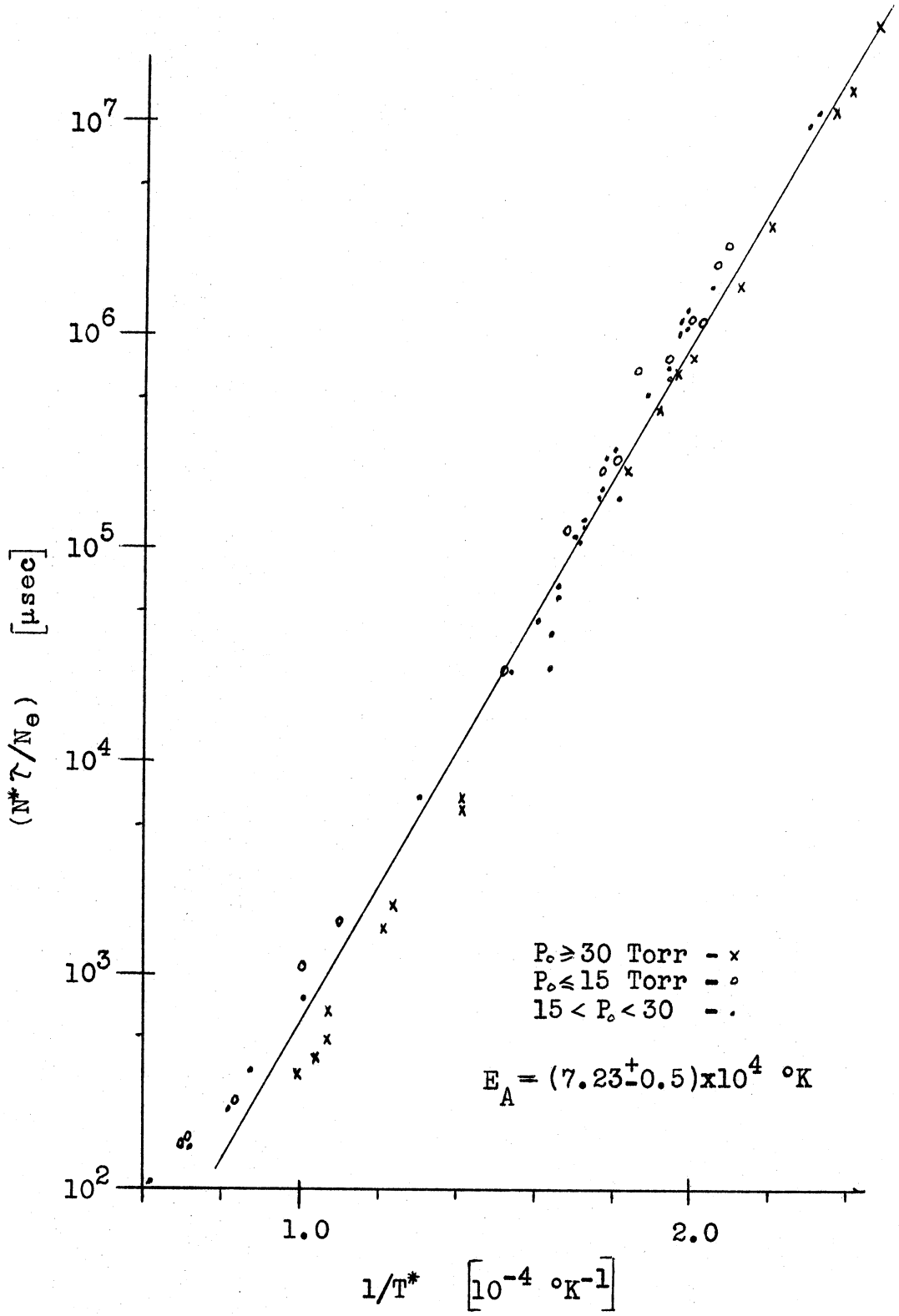

Figure 17. Plot of $\log(N^*\tau/N_e)$ against $1/T^*$ for Mercury.

6. Activation Energy

From Figure 16, we may now say that

$$\tau \doteq C(Ne/N^*) \exp(E_A/T) ,$$

where C is a constant, and E_A apparently varies in the temperature range covered (note change in slope). The activation energy should be the energy of the rate-controlling step of the relaxation reaction, but two collision reactions occur during relaxation which may have different values of E_A . For the high temperature end of Figure 16, where relaxation depends mainly on electron-atom collisions, the slope of the graph gives $E_A = (11.5 \pm 1.0) \times 10^4$ °K, which corresponds quite well with the ionization potential of the mercury atom ($\chi = 12.1 \times 10^4$ °K or 10.43 eV). This result indicates that the electron-atom-dominated relaxation proceeds in a single step rather than by intermediate stages as Kim concluded[6].

The variation in E_A (slope) does not necessarily mean that E_A is temperature dependent. The value obtained will be the average, over the entire τ, of the E_A effective at each instant during relaxation. For the atom-atom collision phase of ionizational relaxation, E_A has been found to correspond to the first excited state of the atom for argon, krypton, xenon[28] and cesium[27]. Thus, E_A from Figure 16 should be slightly low, because the first part of the relaxation must proceed by atom-atom collisions, which depend upon the first excited state of the atom (5.42×10^4 °K or

4.76 eV). For lower temperature shocks (upper end of Fig. 16) the atom-atom process will occupy an increasing fraction of the relaxation, so we expect, and find, even lower values of E_A (= 7.3 x 10^4 °K at the top).

If the N_e dependence is not accepted, then from Figure 13 using only the low P_o points, we may obtain a value for E_A (= 5.2 x 10^4 °K) approximately equal to the energy of the first excited state of the atom. All other values of E_A determined from Figures 11 or 13 are too low--E_A must be equal to, or greater than, the energy of the first excited state of the mercury atom. Values of E_A less than the energy of the the first excited state cannot be explained by impurity effects, since the excited states of most impurities will be above that of the mercury, and the amount of impurity is far too low.

B. Argon

Figures 18 and 19 show the important plots for argon. τ again depends on P_o (N^*) and N_e, and the scatter of experimental points was observed to be less for T than for T^*, as with mercury. From Figure 19, E_A = (11.4 $\pm$ 0.8) x 10^4 °K which is less than the energy of the first excited state of the argon atom (13.4 x 10^4), but approximately equal to the ionization potential of mercury. There may have been appreciable mercury vapor present as an impurity in all argon shocks. It was not realized at the time, but

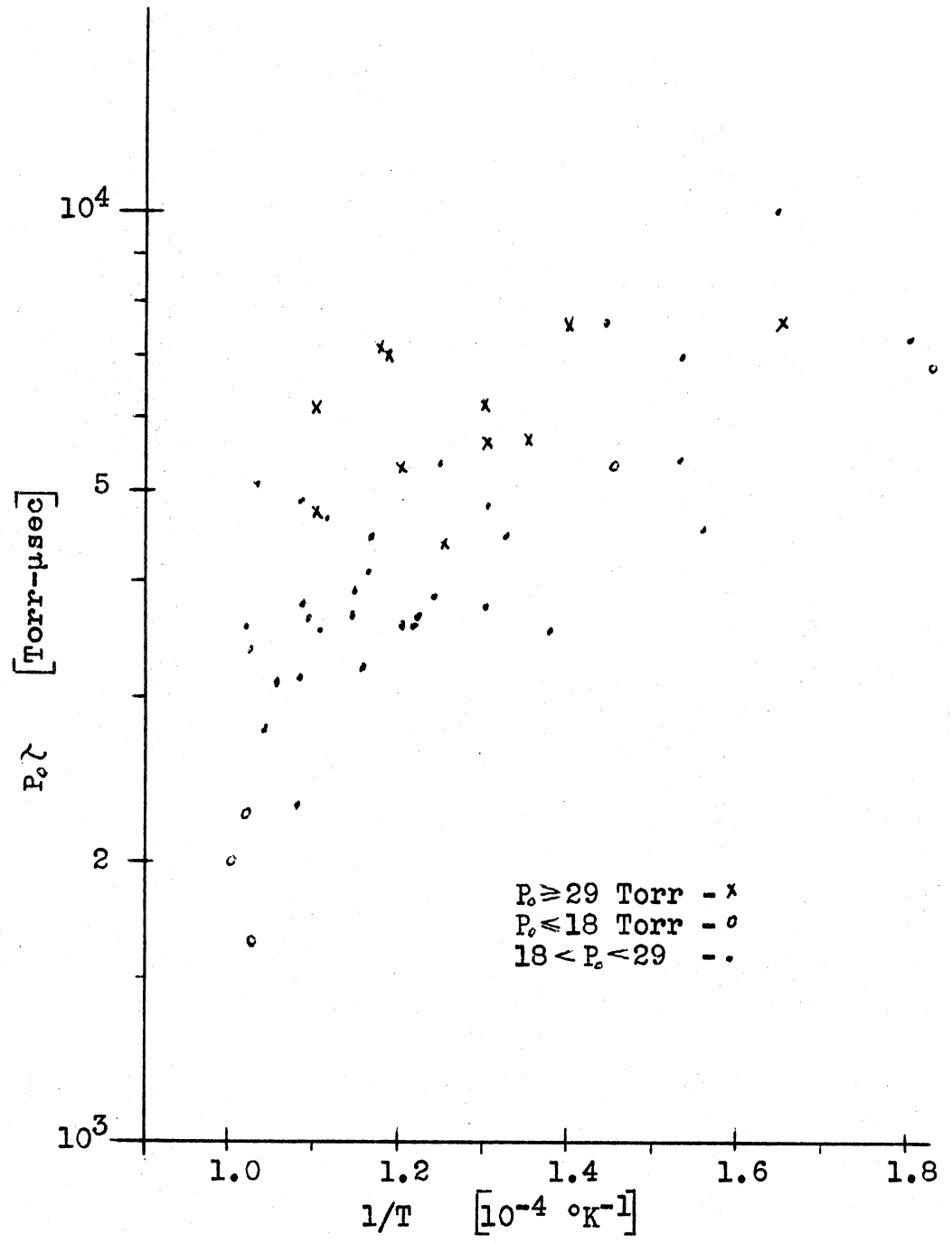

Figure 18. Plot of log $P_o\tau$ against 1/T for Argon.

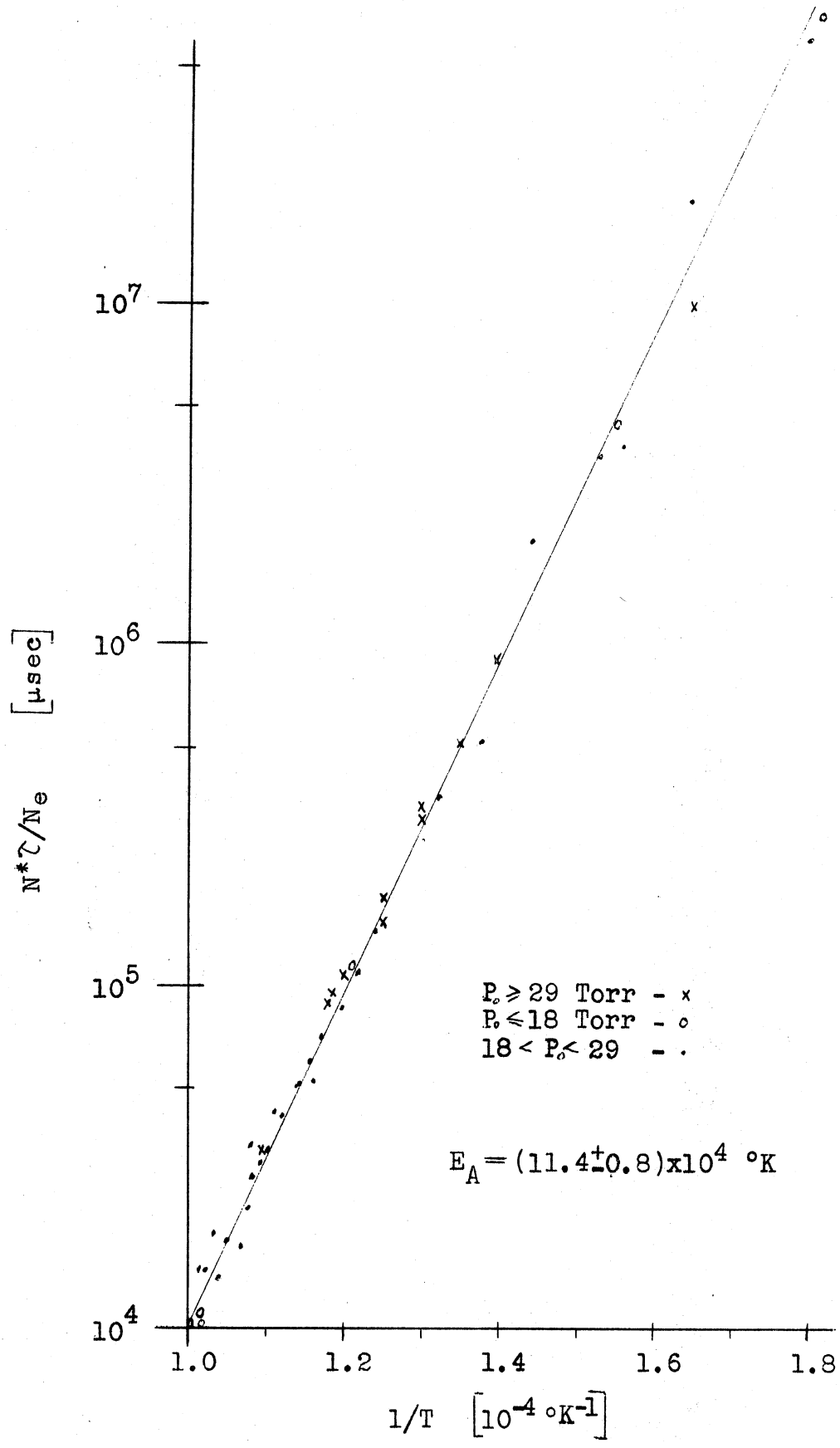

Figure 19. Plot of $\log(N^*\tau/N_e)$ against 1/T for Argon.

if the water cooled trap (between the shock tube and the diffusion pump) was not efficient enough, the mercury diffusion pump might actually maintain several microns of mercury vapor in the heated tube at all times. Therefore, as pointed out by Jones and McChesney[32], the observed E_A should be that for an easily excited impurity, even for quite low impurity concentrations. The fairly high mercury contamination will act as the source of electrons for the argon reaction and the mercury ionization energy will be seen as the effective E_A.

Because of the suspected mercury contamination of all argon shocks, conclusions based solely on the present argon data are not considered reliable.

CHAPTER VI

SPECIAL RESULTS RELATED TO THE LUMINOSITY PROFILE

1. Radiation Decay

Pictures of luminosity traces for three strong mercury shocks are shown in Figure 20. The shape of these curves, agrees extremely well with those of Tumakaev and Lazovskaya[7]. Their curves are actually plots which represent the measured populations of individual mercury atom excited states at various distances behind the shock. The observed total luminosity profile apparently agrees with that due to individual spectral lines--at least for strong shocks.

Tumakaev and Lazovskaya also claim that a considerable number of excited atoms, due to photoexcitation resulting from diffusion of resonance radiation, are present in the mercury vapor ahead of the shock wave. In the present study, very strong luminosity was detected before the arrival of the shock, but whether this was radiation from excited atoms, or light scattered from the walls of the tube, is not known. This pre-luminosity was so great for strong shocks that the original schlieren light source was too faint to be detected and the brighter laser schlieren system was needed. Weymann and Holmes have studied similar pre-luminosity due to electron diffusion[33], and due to photoionization[34], in argon where the effect is considerably smaller than in mercury. In Figure 20 the upper beam trace of M54 clearly shows that the luminosity at window #2 is not zero when the shock

M54

P_o = 12.33 Torr

T = 7636 ^oK

Sweep = 20 μs/cm

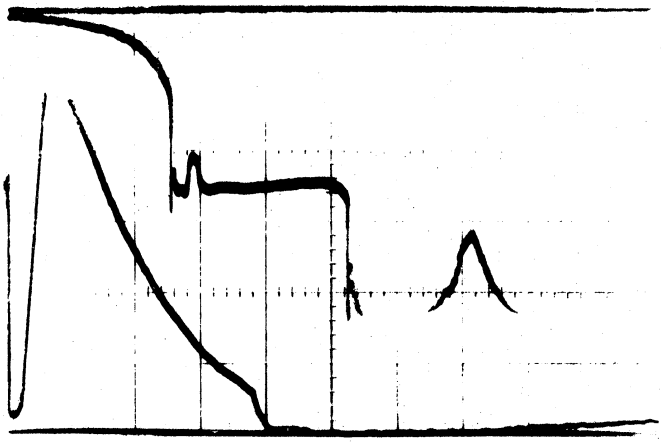

M70

P_o = 15.57 Torr

T = 8471 ^oK

Sweep = 20 μs/cm

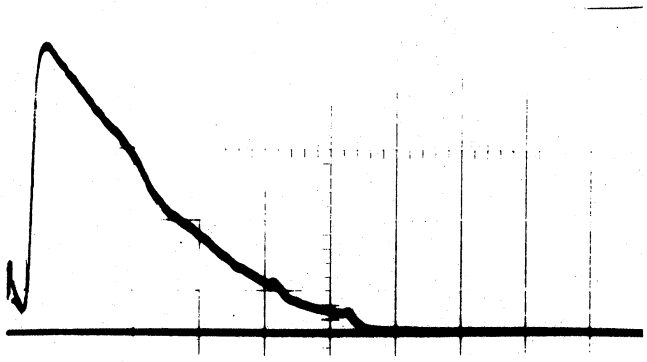

M65

P_o = 37.15 Torr

T = 8004 ^oK

Sweep = 20 μs/cm

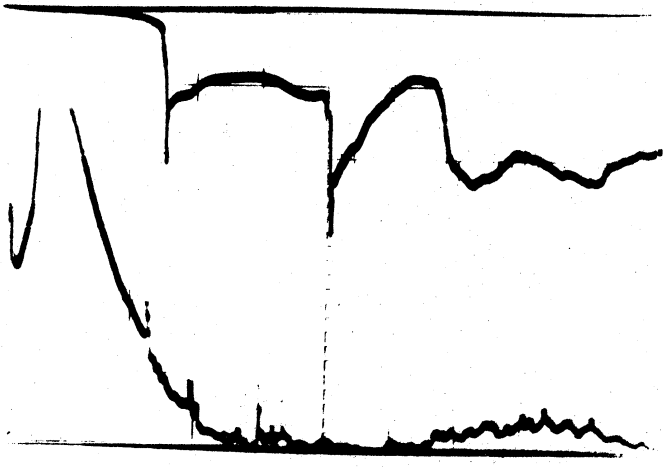

Figure 20. Radiation Decay Curves for Mercury.

arrives.

Kim states[6,25] that boundary layers are very thick for all strong mercury shocks. This would suggest that a large part of the apparent radiation decay may actually be the result of observing the plasma through growing boundary layers. Laminar boundary flows are difficult to detect. With the sensitive laser schlieren system, however, some traces show extra spikes (eg. M65) which can only be from the schlieren system. This indicates that turbulence is present, either in the plasma or in a boundary layer.

During relaxation, radiation decay may be relatively unimportant until the very end (and after), but boundary layers, which absorb material from the plasma, could have a very strong influence on the observed relaxation time. The question of whether the observed luminosity decay is due to boundary layers or radiation decay, could be answered by observing the same strong shock simultaneously through different plasma thicknesses--this is possible with a rectangular tube cross-section. The radiation decay rate would be unaffected, while the ratio of plasma to boundary layer thickness would definitely change.

2. Unusual Features of the Luminosity Profile

The traces of the three different shocks given in Figure 21 demonstrate a rather unexpected luminosity characteristic which is present for both argon and mercury. Each profile contains two distinct points at which the slope of the curve

A10

P_o = 19.73 Torr

T = 8768 ^oK

Sweep = 10 μs/cm

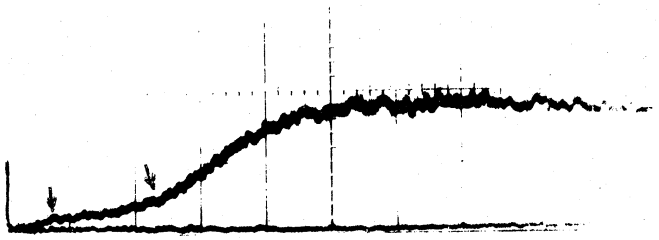

A19

P_o = 14.40 Torr

T ≐ 7500 ^oK

Sweep = 5 μs/cm

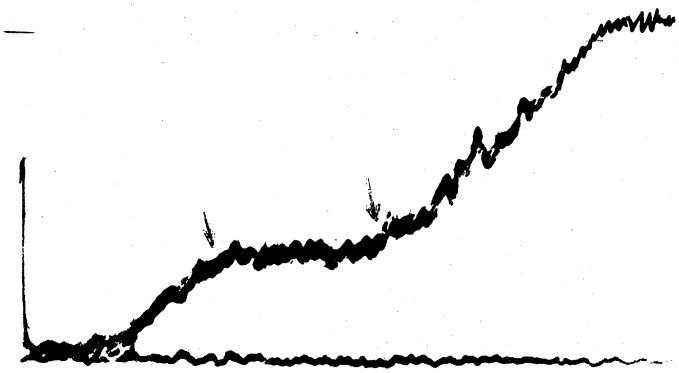

M23

P_o = 14.26 Torr

T = 5839 ^oK

Sweep = 10 μs/cm

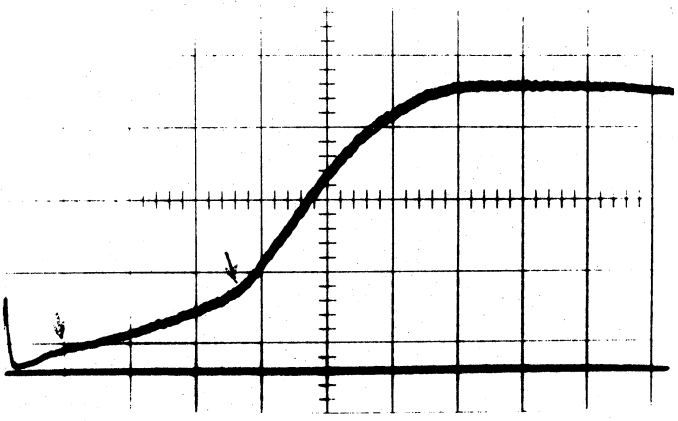

Figure 21. Luminosity Profiles Showing Bends.

changes abruptly. These bends can be seen in all shock traces (except very strong mercury shocks) but are often not as pronounced as in the sample traces. No reason could be found for why the bends are more pronounced in some shocks than in others and the reason for this unusual luminosity feature is not known. A better understanding of this feature and why it occurs may aid in understanding the entire relaxation process.

This feature of relaxation has not been noted previously, possibly because no previous research used this particular method of observing the luminosity. The total luminosity is usually recorded directly on film, with a different spectral range being recorded (usually much further into the U.V.), and much poorer time (space) resolution than the present system. The bends have apparently not been observed for the curves of growth of the electron density during relaxation, using microwave reflection or electron probe techniques. Neither of these techniques, however, can observe the entire relaxation curve efficiently, and again the time resolution is not generally as good as the present system.

Thus we may either assume that this feature is actually present but was obscured by poor resolution in other experiments, or, it is the result of observing a limited and integrated spectral range with the present technique.

The second alternative does not seem likely since the total radiation should increase uniformly during relaxation and there is no apparent reason why one spectral range (or

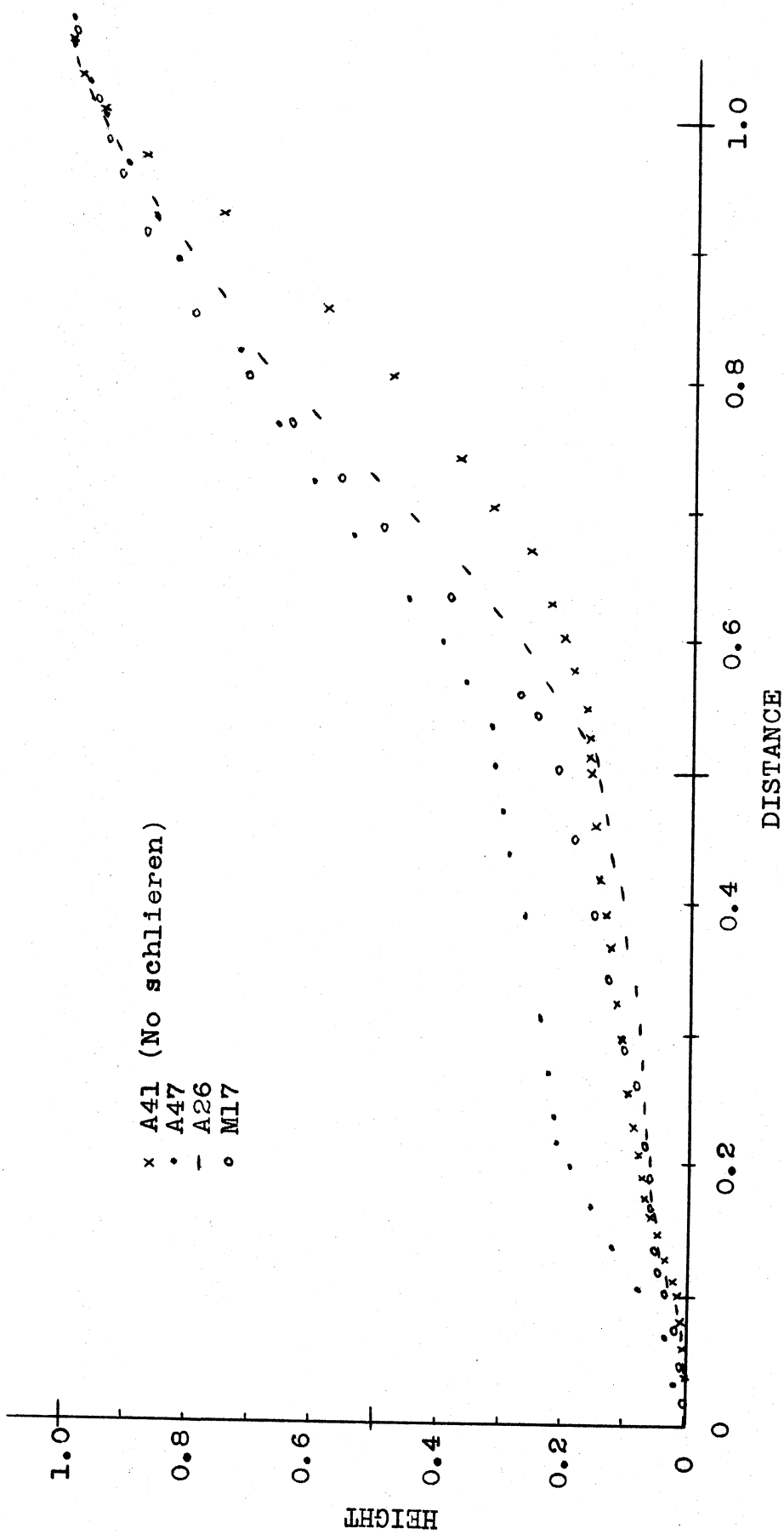

Figure 22. Plots of Normalized Luminosity Profiles

strong line?) should vary differently from the total. This question could be decided by an experiment which would observe the total luminosity and a single spectral line, say the resonance line 2537 A°, simultaneously for comparison.

Some possible experimental causes for the unusual curve shape can be eliminated. Fox, McLaren and Hobson[35] have given the transformation from laboratory to particle time, and their work eliminates the laboratory time scale distortions (much too small) as the source of the unusual shape. Several shock traces, obtained without the presence of any schlieren system still show bends (see Fig. 22), thus eliminating the schlieren system as the cause of this phenomenon.

There are some indications in other research results that this feature is actually present in all shocks. Kelly's[36] Figure 5 does seem to show the same effect for microwave measurements of the electron density in an argon shock. The experimental points of Wong and Bershader[29] vary from their theoretical curves in a manner also slightly suggestive of this same feature. Petschek and Byron[10] briefly observed the argon continuum using a phototube, as verification for their electron probe technique, and although their curves show a great deal of noise fluctuation there is a suggestion of the same bends.

Figure 22 shows the plots for several traces which have been measured and normalized ($\tau = 1$ and maximum height = 1) for comparison. From these graphs, and consideration of the

other traces, it appears that the second bend always occurs between 48% and 55% of the total relaxation time (τ_L). Therefore, the time to the second bend (t_2) satisfies (though not as well) all the same relationships as τ (Figs. 13 and 16). No reasonable relationship could be found between t_1, the time until the first bend occurs, and the plasma variables--perhaps because the measurements of t_1 are not very accurate ($\pm$ 30%).

The time from t_2 to τ_L may correspond to the electron-atom phase of relaxation--Haught[27] indicates that this phase occupies approximately $\frac{1}{2}\tau$. Perhaps t_1 is the time for the atom-atom phase, with t_1 to t_2 representing the region where both collision processes are competing, or an unknown third process exists.

3. Impurity Effects

Figure 23 shows the effect of small amounts of air impurity (deliberately introduced via tube leak) on the mercury luminosity profile. For extremely low impurity levels the characteristic "overshoot" form appears. The luminosity overshoots the final equilibrium value, and then returns to equilibrium shortly later, thus producing a hump at the beginning of the constant luminosity region. In the present research, tests prove that radiation overshoot is definitely a low impurity level effect. For impurity levels below that of M24 (0.005%) no profile deformation occurs. The same form appears in argon but at an impurity level about four times

M24-A

P_o = 15.57 Torr

T = 6070 ^oK

Sweep = 20 μs/cm

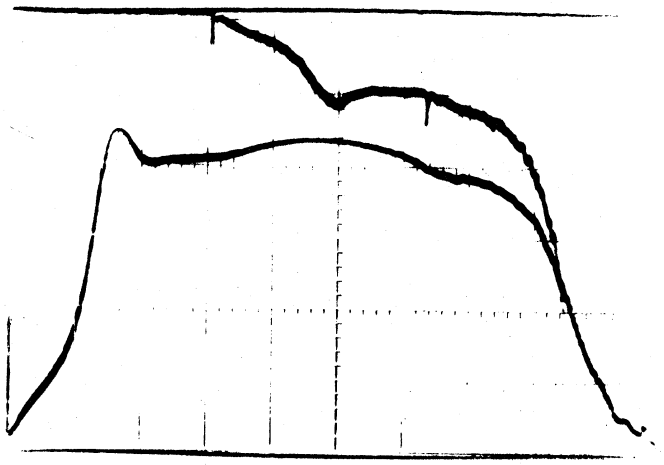

M24-B

Sweep = 10 μs/cm

~0.005% Air

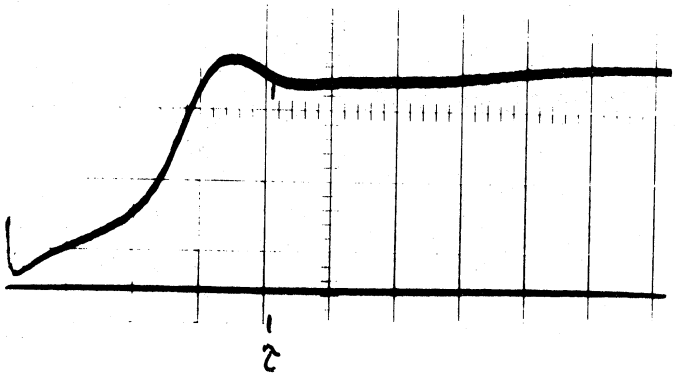

M73

P_o = 16.11 Torr

T = 6288 ^oK

Sweep = 5 μs/cm

~0.02% Air

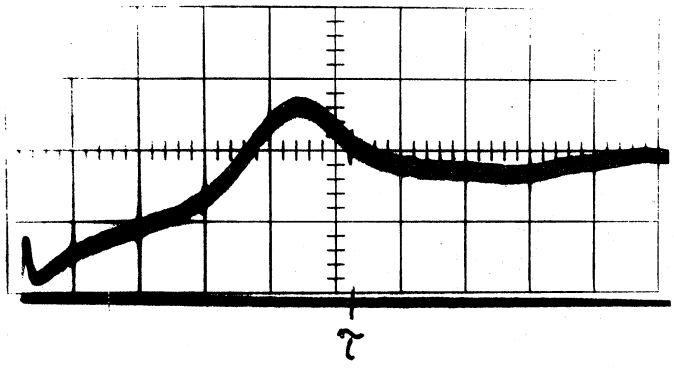

Figure 23. Radiation Overshoot in Mercury.

higher than for mercury. Haught[27] claimed very high gas purity for his study of cesium (<1 part per million), but he observed radiation overshoot for all of his shocks. It would appear that impurities are more important when the first excited state of the atom is lower.

Morgan and Morrison[30] have criticized the use of the luminosity delay time as the relaxation time, mainly on the basis of Haught's luminosity curves. However, the problem is only to decide at which point on the trace the relaxation is actually complete. When the length of the overshoot hump is appreciable relative to τ_i, the best point to use is easily determined. From the traces for several shocks it has been determined that if τ_i is taken as the beginning of the flat region immediately behind the hump then the shock fits extremely well on Figures 13 and 16. This is the same point which Haught arbitrarily chose for his work. τ is still deflined as the time until the luminosity is within 5% of its final asymptotic value.

Figure 24 shows three shock traces from a series taken to demonstrate the effect of impurities on argon--all shocks were approximately the same, except for the amount of impurity. Actually, two series were run, one with hydrogen as the impurity and the other with air, but the two series are indistinguishable. AI-2 has the lowest impurity level which shows an effect--the first hump is overshoot, the second is due to scattered light from the reflected shock. For higher impurity levels the overshoot hump becomes less

Argon
0.02% Air

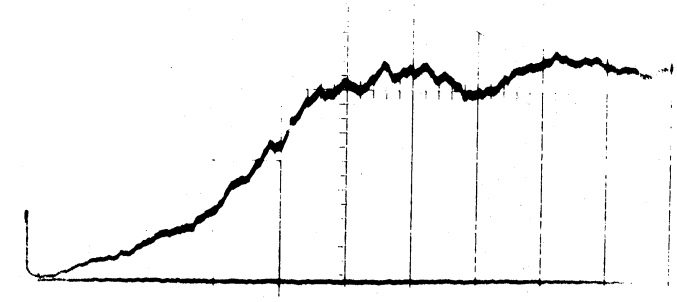

Argon
0.2% Air

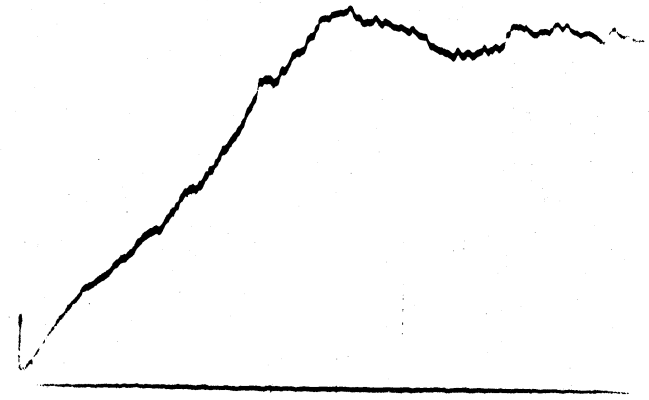

Argon
2.3% Air

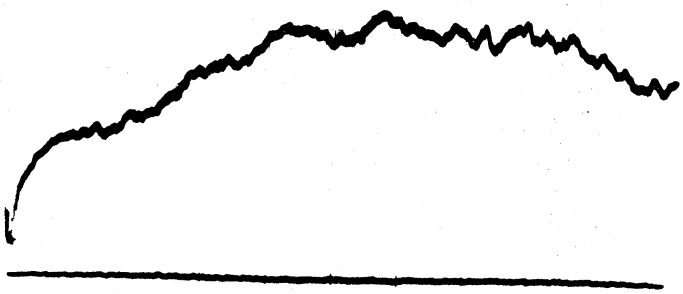

$P_c \doteq 20$ Torr, $T \doteq 7600\ ^{o}K$, Sweep = 10 μs/cm

Figure 24. Air Impurity in Argon.

apparent as the entire profile becomes greatly distorted. Impurities affect the relaxation zone only, although the entire trace seems to become more erratic (noisy) when impurities are present.

Figure 25 shows some types of contamination which could accidently occur. MI-3 demonstrates dibutyl pthalate (D.B.P.) vapor contamination. D.B.P. is used in the manometer for measuring gas pressures. In the present research, the D.B.P. vapor is isolated from the shock tube by the bellows gauge, but if gas pressures are measured directly using an oil manometer, contamination will result. This is extremely important because many researchers use oil manometers for pressure measurements and then claim unusually high gas purity, whereas oil contamination may actually be influencing all of their results.

Small amounts of impurities are often deliberately added to the test gas in order to identify the shock position by a large luminous (molecular) spike. MI-3 shows that the oil molecular spike is actually about 4 μseconds behind the shock (for a strong shock). An error of this size may only be ignored in experiments where τ is very large. The actual time error for a given impurity can only be determined by experiment, and will obviously depend upon the type of impurity used.

AI-10 shows Duo-seal pump oil contamination. At the slower sweep speed no delay is noted for the molecular spike,

AI-10

P_o = 10.60 Torr

T = 6800 ^oK

Sweep = 10 μs/cm

Argon with Pump

Oil Contamination

MI-3

P_o = 12.87 Torr

T = 8563 ^oK

Sweep = 2 μs/cm

Mercury with

D.B.P. Contamination

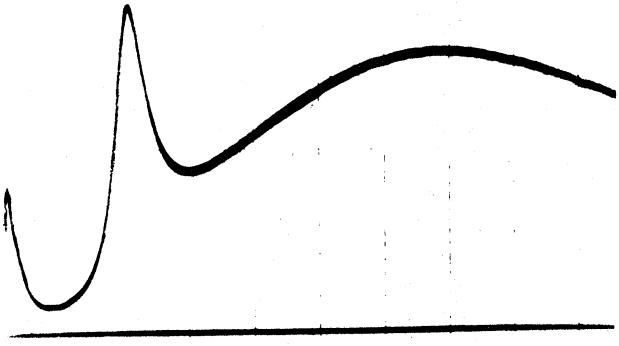

Figure 25. Oil Contamination Profiles.

but the spike at zero time is much too broad to be the schlieren system alone. This particular oil contamination was introduced accidently. When the oil in the Duo-seal pump for the driver section became too low, the oil overheated and oil vapor was introduced into the driver section between shocks. The oil contamination was then carried into the expansion chamber when a shock was fired, and the next shock showed oil contamination.

Noting the contamination associated with two types of oil, an attempt was made to introduce contamination due to a common diffusion pump oil (Convoil-20 Vacuum Pump Fluid). Many shock tubes use oil diffusion pumps instead of mercury. Under no circumstances could any significant affect on the luminosity profile be produced.

The mercury contamination of argon shocks did noticeably affect the luminosity profile but did change the total relaxation time significantly. The same result could also be true of any type of impurity contamination. Mercury impurity in argon did not cause overshoot--perhaps because the ionization potential of mercury is slightly lower than the first excitation level of argon, rather than being higher as in the case of nitrogen or hydrogen impurity.

CHAPTER VII

SUMMARY

Comparison of the point scatter, in the plots of log τ against $1/T^*$ and log $P_o\tau$ against $1/T^*$ for mercury, establishes that ionizational relaxation time depends approximately on P_o^{-1}. The fact that log $(P_o\tau)$ against $1/T$ results in even less scatter demonstrates that for highly ionized relaxations, the final plasma temperature T is more relevant than the commonly used ideal gas temperature T^*. Point scatter is further reduced very slightly in the plot of $\log(P_o\tau/N_e)$ against $1/T$ indicating that ionizational relaxation time is approximately proportional to N_e, the final electron density of the plasma. The inclusion of N_e also results in a more acceptable value for the activation energy.

The value obtained for the activation energy indicates that ionization resulting from electron-atom collisions proceeds as a single step rather than by cumulative steps as in the case of atom-atom collisions.

The above conclusions may also be drawn from the argon data but the value obtained for the activation energy indicates that all argon shocks may contain appreciable mercury as an impurity. For this reason conclusions are not based solely on the argon data.

It is not likely that further research, which compares the total ionizational relaxation times of different shocks,

can contribute significantly to a better understanding of the relaxation process. Future studies of ionizational relaxation should attempt to observe individual shocks in greater detail rather than attempting to relate many different shocks. The ionizational relaxation phenomenon appears to be too complex to be analysed by any one observation technique alone. Each individual shock should be examined simultaneously using several different techniques and the results related if the relaxation processes are ever to be completely understood. There is more information contained in each shock than can be obtained from a single number representing the total relaxation time.

The observed luminosity profiles of the present research show two bends. This is the first time this feature has been observed, probably because of the unusually high spatial resolution of the present observation technique (0.006 inch). The very poor spatial resolution of drum camera techniques (0.150 inch) makes them virtually useless for studying the relaxation process. The reason for the bends in the luminosity profile is not known. The shape of the profile suggests that the total luminosity consists of at least two components which vary differently in form. It is suggested that a future study should compare individual spectral lines with one another, with the continuum and with limited spectral regions, using the present observation techniques. Special attention should be given to the resonance line 2537 A°. It would be helpful to the understanding of re-

laxation processes to know how different spectral regions and lines compare during the relaxation.

For strong shocks in mercury, radiation decay is apparently very pronounced; however, there are indications that part of the observed effect is actually due to boundary layers. The proportion of the effect which is due to boundary layers can be determined by comparing the same shock simultaneously through different plasma thicknesses in a rectangular cross-section tube. If boundary layers are very pronounced then the results of studies in the strong mercury shock region will always be questionable.

Radiation overshoot is a low impurity level effect and the relaxation time, for shocks showing overshoot, appears to correspond to the end of the overshoot hump. Air and hydrogen as impurities appear to greatly affect the shape of the relaxation luminosity profile.

Manometer oil, or pump oil contamination can produce very pronounced changes in the relaxation processes. This is extremely important because it shows the need to guard against these contaminations in all future experiments and also casts doubt on the results of some previous experiments.

APPENDIX

The measured laboratory variables for the relaxation studies of this research are given for future reference. The mercury data are tabulated in Table I, and although the argon shocks are believed to be contaminated by mercury vapor the argon data are tabulated in Table II.

The following laboratory data values are given:

V The shock velocity at window #1, in cm per μsecond. Corrections have been made for the thermal expansion of the tube, and for deceleration in the mercury shocks.

P_o The initial pressure in the tube ahead of the shock, in Torr, was measures in mm of D.B.P. but values have been converted to Torr using the measured density of D.B.P.

T_o The temperature of the tube ahead of the shock, in °C,

τ_L The laboratory relaxation time, in μseconds, is taken as the time from shock passage until the luminosity is within 5% of its final asymptotic value.

t_1 The laboratory time from shock passage until the first bend in the luminosity profile, in μseconds.

t_2 The laboratory time from shock passage until the second bend in the luminosity profile, in μseconds.

Corrections have been made to V, τ_L, t_1 and t_2 for oscilloscope sweep rate differences and non-linearity.

Table 1. Mercury Laboratory Data

Shock	V (cm/sec)	P_o (Torr)	T_o (°C)	λ_i (μsec)	t_1 (μsec)	t_2 (μsec)
M1	111,090	16.57	242	36.8	-	-
M2	103,420	18.19	242	86.7	13	44.3
M3	115,680	16.11	242	30.7	3.8	15.7
M4	111,750	26.05	241	20.0	-	11.3
M6	116,600	10.71	238	38.9	4.9	18.2
M7	108,700	19.34	237	46.8	9.5	27.7
M8	111,090	16.03	242.5	40.6	-	23.5
M9	100,900	16.11	240	94.2	-	-
M10	100,820	16.11	240	95.9	10.7	46.3
M11	97,940	14.18	241	135.1	26.4	67.1
M12	104,420	12.49	241	148.8	19.9	69.3
M13	92,920	20.96	241	110.4	-	59.0
M14	92,470	18.65	241	114.5	-	58.8
M15	107,290	13.87	240.5	81.5	10.8	38.7
M16	99,120	16.49	240	104.1	6.4	50.6
M17	106,140	15.72	240	79.2	10.7	40.1
M18	101,210	18.03	244	97.5	7.4	45.4
M19	109,760	15.49	244	54.6	11.7	30.2
M20	99,850	14.72	245	86.2	7.6	38.7
M21	100,440	14.87	244.5	103.8	7.5	55.9
M22	101.980	14.57	245.5	98.6	12.7	53.7
M23	110,160	14.26	245	67.0	6.4	35.2
M24	112,930	15.67	245	34.6	8.5	16.0
M25	109,070	15.34	244.5	48.4	-	24.9
M26	98,660	14.95	245	126.9	10.7	60.7
M28	89,050	30.83	244	90.4	-	47.8
M29	91,220	30.83	244	61.8	-	-
M30	90,500	30.60	244	60.7	6.4	32.1
M31	95,070	33.60	244	53.1	7.5	28.1
M33	104,940	33.29	252	34.2	5.3	15.7
M35	100,130	34.83	250	44.3	10.7	-
M36	105,830	12.41	246	75.6	5.8	38.5
M38	101,050	32.37	243	46.5	-	22.9
M39	97,130	34.14	242.5	43.4	-	-
M41	111,600	29.05	241	13.05	-	6.8
M42	103,020	31.06	242	49.2	7.5	24.1

Table 1. Mercury Laboratory Data (con't).

Shock	V (cm/sec)	P_o (Torr)	T_o (°C)	τ_i (μsec)	t_1 (μsec)	t_2 (μsec)
M43	105,630	29.29	242	28.6	-	-
M45	94,850	15.88	242	137.1	-	59.9
M46	100,880	17.26	242	93.7	-	60.1
M47	101,970	15.41	242	85.2	6.4	40.8
M48	107,000	15.26	240	83.3	4.4	43.2
M49	101,910	16.65	240	71.2	6.4	38.3
M50	107,150	16.18	240	60.8	-	-
M51	107,480	15.57	240	64.3	11.0	35.8
M52	108,740	16.03	242	53.7	6.6	28.1
M53	126,290	15.41	242	20.5	-	12.0
M54	138,370	12.33	242	10.57	-	4.8
M55	145,540	11.71	242	8.49	-	4.3
M56	160,270	12.87	242	4.16	-	2.0
M57	173,390	11.87	242	2.85	-	-
M58	173,730	12.72	242	2.75	-	-
M59	129,770	30.98	243	6.43	-	-
M60	131,090	32.98	243	5.33	-	-
M61	120,680	31.14	243	9.28	-	-
M62	120,690	32.52	243	9.87	-	-
M63	140,350	30.52	243	3.76	-	-
M64	141,530	41.00	242	2.23	-	-
M65	140,410	37.15	242	2.45	-	-
M66	144,630	41.46	240	2.12	-	-
M67	161,660	22.20	240	2.75	-	-
M68	172,890	18.34	238	2.65	-	-
M69	187,880	17.57	240	1.925	-	-
M70	156,130	15.57	240	3.54	-	-
M71	144,490	16.03	240	5.78	-	-

Table 2. Argon Laboratory Data

Shock	V (cm/sec)	P_o (Torr)	T_o (°C)	τ_i (μsec)	t_1 (μsec)	t_2 (μsec)
A1	296,580	19.22	198	44.8	6.3	23.0
A2	340,470	9.43	198	39.9	9.0	21.0
A3	293,680	18.65	198	49.1	8.9	24.2
A4	320,550	21.42	198	44.2	9.1	18.9
A5	315,520	21.12	195	42.0	9.9	23.2
A6	305,440	21.42	195	38.5	5.6	21.5
A7	282,400	21.50	200	54.8	12.7	23.4
A8	236,700	23.35	197	52.7	-	-
A9	299,820	19.53	197	47.4	7.5	26.6
A10	309,040	19.73	197	47.0	5.6	25.0
A11	313,060	21.12	197	46.4	8.4	24.1
A12	318,850	19.88	197	45.9	8.8	21.6
A13	327,520	19.34	198	39.0	11.4	19.3
A14	332,030	18.80	198	35.5	11.4	18.7
A15	336,570	18.22	163	43.4	-	21.0
A16	337,510	18.80	165	45.0	11.2	20.6
A17	304,270	27.74	164	41.0	11.9	22.2
A18	319,610	26.20	165	46.4	10.9	21.8
A20	338,460	14.80	167	35.3	11.0	20.7
A21	344,260	13.26	167	34.1	-	-
A22	313,780	27.51	166	42.7	11.3	21.8
A24	305,820	26.51	162	28.1	5.8	16.0
A25	322,690	19.27	163	29.2	2.3	13.2
A26	297,660	16.65	163	46.2	6.0	21.8
A27	276,990	19.88	163	51.7	-	28.1
A29	237,940	17.73	163	65.5	-	32.4
A30	240,030	19.19	162.5	51.1	-	27.3
A31	259,710	17.65	162	62.0	-	-
A32	251,590	18.80	160	142.8	45.4	81.5
A33	261,350	19.96	160	71.8	-	-
A34	258,840	21.19	162	57.3	-	25.5
A37	270,340	20.11	161	249.0	-	113.5
A39	286,210	29.36	162	50.3	9.9	24.8
A40	292,460	29.13	161	40.0	11.2	19.0
A41	279,560	32.29	160	46.7	6.7	21.8
A42	275,100	39.30	160.5	50.0	6.3	28.0

Table 2. Argon Laboratory Data (con't).

Shock	V (cm/sec)	P_o (Torr)	T_o (°C)	τ_i (μsec)	t_1 (μsec)	t_2 (μsec)
A44	285,260	21.58	162	45.0	7.0	24.5
A46	322,170	21.89	162.5	35.5	8.6	-
A47	298,990	32.29	161.5	42.7	9.2	23.8
A54	301,490	40.69	254	45.6	10.5	23.1
A56	331.310	26.67	254	46.3	-	25.1
A57	315,700	29.05	255	41.3	6.2	21.2
A58	299,390	46.09	254	40.2	5.5	21.0
A59	249,680	38.15	252.5	54.1	3.9	23.8

REFERENCES

1. Laporte, O., Scientific American, December 1949, pp. 14-19.

2. Mautz, C.W., Geiger, F.W., and Epstein, H.T., "On the Investigation of Supersonic Flow Patterns by Means of the Shock Tube", Phys. Rev., Vol. 74, No. 12, 1872-3, (1948).

3. Penner, S.S., "The Determination of Absolute Intensities and f-Numbers from Shock Tube Studies", Technical Report 5, California Institute of Technology, Jet Propulsion Laboratory (1957).

4. Turner, E.B., Ph.D. Thesis, Univ. of Michigan. (1956).

5. Hill, R.A. and Gerardo, J.B., Phys. Rev. Vol. 162, No.45 (1967).

6. Kim, Y.W., "Ionized Mercury Gas in the Heated Shock Tube: The Measurement of Relaxation Times and Absolute Intensities", Ph.D. Thesis, Univ. of Michigan (1968).

7. Tumakaev, G.K. and Lazovskaya, V.R., "Investigation of the State of Mercury Vapor in a Shock Tube by the Rozhdestvenskii Hook Method", Soviet Physics--Technical Physics, Vol. 9, No. 10, 1499-55, (1965).

8. Stupochenko, Y.V., Losev, S.A. and Osipov, A.I., "Relaxation in Shock Waves", (1965), English Translation by Springer-Verlag Press, N.Y., (1967).

9. Yoder, M.J., "A Cryogenic Shock Tube: Low Temperature Shock Waves in Molecular Hydrogen", Ph.D. Thesis, Univ. of Michigan (1971).

10. Petschek H. and Byron, S., "Approach to Equilibrium Ionization behind Strong Shock Waves in Argon", Annals of Physics, Vol. 1, 270-315 (1957).

11. Dunaev, Y.A., Tamakaev, G.K., Zhikhareva, T.V., and Lasovskaya, V.R., "Kinetics of Ionization and Excitation of Mercury Atoms Ahead of and Behind the Shock Front" Paper 33, 8th International Shock Tube Symposium, London (1971).

12. Laporte, O., "High Temperature Shock Waves", Combustion and Propulsion, Third AGARD Colloquium (Pergamon Press, New York), p 499 (1958).

13. Courant, R. and Friedrichs, K.O., "Supersonic Flow and Shock Waves", Ch. 1 (Interscience, New York, 1948).

14. Kim, Y.W., "Generalization of Reflected Shock Calculations" Phys. of Fluids Vol. 14, 6, p 1280 (1971).

15. Wilkerson, T.D., "The Use of the Shock Tube as a Spectroscopic Source with an Application to the Measurement of gf-Values for Lines of Neutral and Singly Ionized Chromium", Ph.D. Thesis, University of Michigan (1961).

16. Mohler, F., Astrophysics Journal, Vol. 90, 429 (1939).

17. Moore, C.E., "Atomic Energy Levels", NBS Circular 467 (1958).

18. Inglis, D.R. and Teller, E., Astrophysics Journal, Vol. 90, 439 (1939).

19. Debye, P. and Hückel, E., Physik. Zeitschr. Vol. 24, 187 (1923).

20. McChesney, M., "Equilibrium Shock-Wave Calculations in Inert Gas, Multiply Ionized Debye-Huckel Plasmas", Canadian Journal of Physics, Vol 42 (1964).

21. Ecker, G. and Kröll, W., Physics of Fluids, Vol. 6, 62 (1963).

22. Kim, Y.W. and Laporte, O., "Construction of a Shock Tube for Metallic Vapors", Shock Tube Symposium, Physics of Fluids Supplement I. (1962).

23. Dell, J.H., "Heated Shock Tube Modifications", Technical Report to Air Force Office of Scientific Research, University of Michigan (1971). (unpublished)

24. Wheeler, W.P. and Coulder, M., "Varian Flanges", Vacuum Symposium Transactions. (1962).

25. Kim, Y.W., Private communications (1970-71).

26. Ladenburg, R.W., et al, editors, "High Speed Aerodynamics and Jet Propulsion", Vol. 9, Princeton University Press, pp. 26-46 (1954).

27. Haught, A.F., "Shock-Tube Investigation of the Ionization of Cesium Vapor", Physics of Fluids, Vol. 5, No. 11. (1962).

28. Harwell, K.E. and Jahn, R.G., "Initial Ionization Rates in Shock-Heated Argon, Krypton and Xenon". Physics of Fluids, Vol. 7, No. 2. (1964)

29. Wong, H. and Bershader, D., "Thermal Equilibrium behind and Ionizing Shock", Journal of Fluid Mechanics, Vol. 26, Part 3. (1966).

30. Morgan, E.J. and Morrison, R.D., "Ionization Rates behind Shock Waves in Argon", Physics of Fluids, Vol. 8, No. 9. (1965).

31. Fowler, R.H. and Guggenheim, E.A., "Statistical Thermodynamics", Cambridge University Press. Chap. 12. (1939).

32. Jones, N.R. and McChesney, M., "Ionization Relaxation in Slightly Impure Argon", Nature, Vol. 209. (March 1966).

33. Weymann, H.D., "Precursors Ahead of Shock Waves: I. Electron Diffusion", Physics of Fluids, Vol. 12, No. 6. (1969)

34. Holmes, L.B. and Weymann, H.D., "Precursors Ahead of Shock Waves: II. Photoionization", Physics of Fluids, Vol. 12, No. 6. (1969).

35. Fox, J.N., McLaren, I.I. and Hobson, R.M., Physics of Fluids, Vol. 9. (1966).

36. Kelly, A.J., Journal of Chemical Physics, Vol. 45, No. 5. (1966).

Unclassified

Security Classification

DOCUMENT CONTROL DATA - R & D

(Security classification of title, body of abstract and indexing annotation must be entered when the overall report is classified)

1. ORIGINATING ACTIVITY (Corporate author)	2a. REPORT SECURITY CLASSIFICATION
The University of Michigan Ann Arbor, Michigan	Unclassified
	2b. GROUP N/A

3. REPORT TITLE

Ionizational Relaxation in Shock-Heated Mercury Vapor

4. DESCRIPTIVE NOTES (Type of report and inclusive dates)

Final Report

5. AUTHOR(S) (First name, middle initial, last name)

James H. Dell

6. REPORT DATE	7a. TOTAL NO. OF PAGES	7b. NO. OF REFS
January 1972	100	36

8a. CONTRACT OR GRANT NO.	9a. ORIGINATOR'S REPORT NUMBER(S)
Grant No. AF-AFOSR-70-1849 b. PROJECT NO.	032150-F-1
c.	9b. OTHER REPORT NO(S) (Any other numbers that may be assigned this report)
d.	

10. DISTRIBUTION STATEMENT

11. SUPPLEMENTARY NOTES	12. SPONSORING MILITARY ACTIVITY
	AF Office of Scientific Research 1400 Wilson Blvd. Arlington, Virginia 22209

13. ABSTRACT

A uniformly heated, pressure-driven shock tube was used to produce 4200 K to 12,000 K mercury plasmas in which the relaxation process was studied. The total plasma luminosity was observed using a photomultiplier tube, with the time of shock passage and shock velocity established using a schlieren optical system.

It is shown that the ionizational relaxation time depends inversely on the initial vapor pressure or atom number density, and directly on the final electron number density. The final plasma temperature is shown to be more relevant for strongly ionized shocks than the commonly used ideal gas temperature.

Ionizations caused by electron-atom collisions appear to occur as a single step rather than by cumulative steps as atom-atom ionizations.

A previously unobserved feature of ionizational relaxation has been detected. The luminosity profile shows two distinct points at which the slope of the curve changes abruptly. No explanation of this feature could be found.

Radiation overshoot is shown to be an effect which occurs at low impurity levels. The true relaxation time corresponds to the end of the overshoot phenomenon. Impurities are seen to affect the shape of the relaxation profile greatly, and manometer and vacuum pump oils are shown to be possible sources of impurity in some previous studies.

DD FORM 1 NOV 65 1473

Unclassified

Security Classification

14 KEY WORDS	LINK A		LINK B		LINK C	
	ROLE	WT	ROLE	WT	ROLE	WT
Heated shock tube						
Mercury plasma						
Ionizational relaxation						
Pressure dependence						
Temperature dependence						
Electron density						
Luminosity profile						